

Extreme value methods for estimating rare events in Utopia

L. M. André¹, R. Campbell², E. D’Arcy¹, A. Farrell², D. Healy³, L. Kakampakou^{2,*}, C. Murphy¹, C. J. R. Murphy-Barltrop^{4,5} and M. Speers¹

¹STOR-i Centre for Doctoral Training, Lancaster University LA1 4YR, United Kingdom

²Department of Mathematics and Statistics, Lancaster University LA1 4YF, United Kingdom

³Hamilton Institute, Maynooth University, Maynooth, Co. Kildare, Ireland

⁴Technische Universität Dresden, Institut Für Mathematische Stochastik, Helmholtzstraße 10, 01069 Dresden, Germany.

⁵Center for Scalable Data Analytics and Artificial Intelligence (ScaDS.AI) Dresden/Leipzig, Germany

*Correspondence to: l.kakampakou1@lancaster.ac.uk

December 18, 2023

Abstract

To capture the extremal behaviour of complex environmental phenomena in practice, flexible techniques for modelling tail behaviour are required. In this paper, we introduce a variety of such methods, which were used by the Lancopula Utopiversity team to tackle the data challenge of the 2023 Extreme Value Analysis Conference. This data challenge was split into four sections, labelled C1-C4. Challenges C1 and C2 comprise univariate problems, where the goal is to estimate extreme quantiles for a non-stationary time series exhibiting several complex features. We propose a flexible modelling technique, based on generalised additive models, with diagnostics indicating generally good performance for the observed data. Challenges C3 and C4 concern multivariate problems where the focus is on estimating joint extremal probabilities. For challenge C3, we propose an extension of available models in the multivariate literature and use this framework to estimate extreme probabilities in the presence of non-stationary dependence. Finally, for challenge C4, which concerns a 50 dimensional random vector, we employ a clustering technique to achieve dimension reduction and use a conditional modelling approach to estimate extremal probabilities across independent groups of variables.

Keywords: Non-stationary Extremes, Extremal Dependence, Generalised Additive Modelling

1 Introduction

This paper details an approach to the data challenge organised for the Extreme Value Analysis (EVA) 2023 Conference. The objective of the challenge was to estimate extremal probabilities, or their associated quantiles, for simulated environmental data sets for various locations on a fictitious planet called Utopia. The data challenge is split into 4 challenges; challenges C1 and C2 focus solely on the univariate setting, whereas challenges C3 and C4 concern multivariate data sets, i.e., we use data from single and multiple locations, respectively.

Challenge C1 requires estimation of the 0.9999-quantile of the distribution of the environmental response variable Y conditional on a covariate vector \mathbf{X} , for 100 realisations of covariates. To do so, we model the tail of $Y \mid \mathbf{X} = \mathbf{x}$ using a generalised Pareto distribution (GPD; Pickands, 1975) and employ the extreme value generalised additive modelling (EVGAM) framework, first introduced by Youngman (2019), to account for the non-stationary data structure. We consider a variety of model formulations and select our final model using cross-validation (CV). Furthermore, 50% bootstrap confidence intervals are estimated, and the final model performance is assessed using the number of times the true conditional quantile lies in the confidence intervals (Rohrbeck et al., 2023). For challenge C2, we are required to estimate the T -year return level for the marginal distribution of Y . In other words, we are interested in the value q satisfying $\Pr(Y > q) = 1/(300T)$, such that $T = 200$.

Challenges C3 and C4 concern the estimation of probabilities for extreme multivariate regions. Such estimates require techniques for modelling and extrapolating within the joint tail. For challenge C3, three unknown non-stationary environmental variables are provided, and we are required to estimate two joint tail probabilities. To achieve this, we propose a non-stationary extension of the model introduced by Wadsworth and Tawn (2013). Lastly, for challenge C4, we wish to estimate the probability that 50 environmental variables jointly exceed prespecified extreme thresholds. To simplify the analysis, we separate the variables into five independent

groups, and obtain separate probabilities for each group using the conditional extremes approach of Heffernan and Tawn (2004).

The remainder of the paper is structured as follows. A suitable background on EVA is introduced in Section 2. Section 3 covers all aspects of the univariate challenges C1 and C2; we outline our exploratory data analysis (EDA) and detail our methodology based on EVGAM, introducing tools for model selection and comparison. In Section 4 we cover the first multivariate challenge C3. After establishing the presence of non-stationarity in the underlying data through EDA, we detail our extension of the Wadsworth and Tawn (2013) model, alongside inferential techniques for this extended framework. Given this non-stationarity, an overview of quantile regression and model fitting is presented. Challenge C4 is covered in Section 5. Given the high-dimensional nature of this problem, our data analysis provides the basis for clustering the variables into independent subgroups, and the conditional extremes approach is used to approximate probabilities for each subgroup. The paper ends with a discussion of the results of all challenges.

2 EVA background

2.1 Univariate modelling

Univariate EVA methods are concerned with capturing the tail of a distribution, allowing extreme quantities to be estimated. The most common univariate approach is the peaks-over-threshold framework. Consider a continuous, independent and identically distributed (IID) random variable Y with distribution function F and upper endpoint $y^F := \sup\{y : F(y) < 1\}$. Pickands (1975) shows that, for some high threshold $v < y^F$, the excesses $(Y - v) \mid Y > v$, after suitable rescaling, converge in distribution to a GPD as $v \rightarrow y^F$. In practice, this limit is taken to hold exactly for an

appropriately chosen high threshold v such that

$$\Pr(Y > y + v \mid Y > v) = \begin{cases} (1 + \xi y / \sigma)_+^{-1/\xi} & \text{if } \xi \neq 0, \\ \exp(-y / \sigma) & \text{if } \xi = 0, \end{cases}$$

for $y > 0$, $w_+ = \max(w, 0)$, shape parameter $\xi \in \mathbb{R}$ and threshold-dependent scale parameter $\sigma > 0$. Note that the case when $\xi = 0$ is taken in the limit as $\xi \rightarrow 0$. We write $(Y - v) \mid Y > v \sim \text{GPD}(\sigma, \xi)$. For $\xi < 0$, the distribution has a finite upper end-point at $v - \sigma / \xi$ but is unbounded above for $\xi \geq 0$. Davison and Smith (1990) provide an overview of the properties of the GPD, and also propose an extension of this framework to the non-stationary setting. Given a non-stationary process Y with associated covariate(s) \mathbf{X} , they propose the following model

$$\Pr(Y > y + v \mid Y > v, \mathbf{X} = \mathbf{x}) = \left(1 + \frac{y \xi(\mathbf{x})}{\sigma(\mathbf{x})}\right)_+^{-1/\xi(\mathbf{x})},$$

for $y > 0$, where $\sigma(\cdot), \xi(\cdot)$ denote functions of the covariate(s). Recent extensions of the Davison and Smith (1990) framework include allowing the threshold to be covariate-dependent, i.e., $v(\mathbf{x})$ (Kysely et al., 2010; Northrop and Jonathan, 2011), and capturing the covariate functions in a flexible manner using generalised additive models (GAMs; Chavez-Demoulin and Davison, 2005; Youngman, 2019).

2.2 Extremal dependence measures

In addition to capturing modelling marginal tail behaviours, multivariate EVA methods are concerned with quantifying the dependence between extremes of multiple observations. An important classification of this dependence, is obtained through the measure χ (Joe, 1997): given a d -dimensional random vector \mathbf{X} , with $d \geq 2$ and $X_i \sim F$ for all $i \in \{1, \dots, d\}$, consider the probability

$$\chi(u) := \frac{\Pr(F(X_i) > u, i \in A \subseteq \{1, \dots, d\})}{1 - u}, \quad |A| \geq 2, \quad (2.1)$$

where $|\cdot|$ denotes set cardinality. Where the limit exists, we set $\chi := \lim_{u \rightarrow 1} \chi(u) \in [0, 1]$. When $\chi > 0$, we say that the variables exhibit asymptotic dependence, i.e., can take their largest values

simultaneously, with the strength of dependence increasing as χ approaches 1. If $\chi = 0$, the variables cannot all take their largest values together. In particular, for $d = 2$, we refer to the case $\chi = 0$ as asymptotic independence.

We also consider the coefficient of tail dependence proposed by Ledford and Tawn (1996). Using the formulation given in Resnick (2002), let

$$\eta(u) := \frac{\log(1-u)}{\log P(F(X_i) > u, i \in A \subseteq \{1, \dots, d\})}.$$

When the limit exists, we set $\eta := \lim_{u \rightarrow 1} \eta(u) \in (0, 1]$. The cases $\eta = 1$ and $\eta < 1$, correspond to cases $\chi > 0$ and $\chi = 0$, respectively. For $\eta < 1$, this coefficient quantifies the form of dependence for random vectors that do not take their largest values simultaneously.

Since χ and η are limiting values, they are unknown in practice and must be approximated using numerical techniques. Therefore, when quantifying extremal dependence, we approximate χ (η) using empirical estimates of $\chi(u)$ ($\eta(u)$) for some high threshold u . See Murphy-Barltrop et al. (2023) for a detailed example.

3 Challenges C1 and C2

This section discusses our approach for challenges C1 and C2 in the univariate setting. Both challenges concern 70 years of daily data for the capital city of Amaurot. Each year has 12 months of 25 days and two seasons (season 1 for months 1-6, and season 2 for months 6-12). Suppose Y is an unknown response variable, and $\mathbf{X} = (V_1, \dots, V_8)$ is a vector of covariates, (V_1, V_2, V_3, V_4) denoting unknown environmental variables and (V_5, V_6, V_7, V_8) denoting season, wind direction (radians), wind speed (unknown scale), and atmosphere (recorded monthly), respectively.

For C1, we build a model for $Y \mid \mathbf{X}$ and estimate the 0.9999-quantile, with associated 50% confidence intervals, for 100 different covariate combinations denoted \mathbf{x}_i for $i \in \{1, \dots, 100\}$. Note \mathbf{x}_i are not covariates observed within the data set, but new observations provided by the challenge organisers.

For C2, we estimate the marginal quantile q such that $\Pr(Y > q) = (6 \times 10)^{-4}$, which corresponds to a once in 200 year event in the IID setting. Therefore, we first estimate the marginal distribution $F_Y(y)$ using Monte-Carlo techniques; see for instance, Eastoe and Tawn (2009). Since we have a large sample size $n = 21,000$ it is reasonable to assume that the observed covariate sample is representative of \mathbf{X} . We can approximate the marginal distribution as follows,

$$\hat{F}_Y(y) = \int_{\mathbf{X}} F_{Y|\mathbf{X}}(y | \mathbf{x}) f_{\mathbf{X}}(\mathbf{x}) d\mathbf{x} \approx \frac{1}{n} \sum_{t=1}^n F_{Y_t|\mathbf{X}_t}(y_t | \mathbf{x}_t). \quad (3.1)$$

To approximate $F_Y(y)$, we first re-estimate the GPD parameters, now using a penalised log-likelihood which incorporates the following loss function, provided by the challenge organisers,

$$\mathcal{L}(q, \hat{q}) = \begin{cases} 0.9(0.99q - \hat{q}) & \text{if } 0.99q > \hat{q}, \\ 0 & \text{if } |q - \hat{q}| \leq 0.01q, \\ 0.1(\hat{q} - 1.01q) & \text{if } 1.01q < \hat{q}, \end{cases} \quad (3.2)$$

where q and \hat{q} are the true and estimated marginal quantiles, respectively. This loss function penalises under-estimation more heavily than an over-estimation.

We conduct the same EDA for both challenges given the same covariates are used; this is outlined in Section 3.1. In Section 3.2 we introduce our techniques for modelling $Y | \mathbf{X}$, which is then used for modelling Y via (3.1). Our approach for uncertainty quantification is outlined in Section 3.3, and we give our results for both challenges in Section 3.4.

3.1 Exploratory data analysis

This section details our exploratory analysis for challenges C1 and C2. We are informed that the response variable Y_t , $t \in \{1, \dots, n\}$, is independent over time (Rohrbeck et al., 2023), but is affected by the covariate vector $\mathbf{X}_t = \{V_{1,t}, \dots, V_{8,t}\}$. However, it is not clear which covariates affect Y , and what form these covariate-response relationships take. In what follows, we aim to explore these relationships so we can account for them in our modelling framework.

To begin, we explore the dependence between all variables to understand the relationships between covariates, as well the relationships between individual covariates and the response variable. We investigate dependence in the main body of the data using Kendall’s τ measure, while for the joint tails, we use the pairwise extremal dependence coefficients χ and η defined in Section 2; values for all pairs are shown in Figure 1, with threshold u set at the empirical 0.95-quantile for the extremal measures.

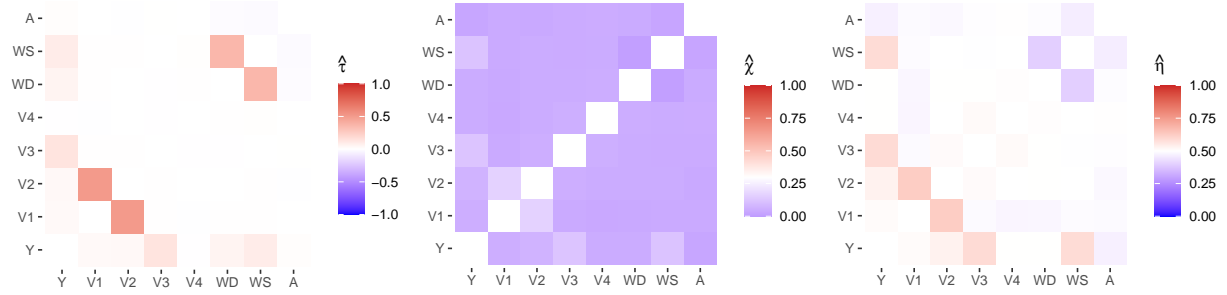


Figure 1: Heat maps for dependence measures for each pair of variables: Kendall’s τ (left), χ (middle) and η (right). Note the scale in each plot varies, depending on the support of the measure, and the diagonals are left blank, where each variable is compared against itself.

The response variable Y has the strongest dependence with V_3 in the body of the distribution, followed by V_6 (wind speed) then V_7 (wind direction). Similarly, Y has strong dependence with V_2 , V_3 and V_6 in the tail. We also find strong dependence between V_6 and V_7 in the body, but evidence of weak dependence in the tail (dark blue for $\hat{\chi}$ and $\hat{\eta}$). There is also strong dependence between V_1 and V_2 in both the body and tail (see dark red for $\hat{\eta}$). We find very similar dependence relationships when the data are split into seasons. In the Supplementary Material, we show scatter plots of each covariate against the response variable; these demonstrate a highly non-linear relationship for each explanatory variable with Y .

Since V_6 and V_7 have strong relationships with the response variable Y , we explore these variables in more detail. The most notable feature of both variables is that they have a significant shift in distribution. We use the changepoint package (Killick and Eckley, 2014) in R to estimate the

difference in mean for both variables; just 5 observations separate the estimated changepoints, so we assume the changes occur simultaneously. Before the changepoint, winds typically occur in the southwest direction and are greater in magnitude, while after the changepoint, they occur mainly in the northeast direction and are lower in magnitude; see the Supplementary Material. Rohrbeck et al. (2023) state this non-stationarity was created unintentionally when designing the data challenge.

Next, we explore temporal relationships for the response variable Y . We first find temporal non-stationarity in that the distribution of Y varies significantly with V_5 (season); see the Supplementary Material for more detail. The magnitude of Y_t is higher for season 1 than season 2, in both the main body and tail of the distribution. However, within each season, across months, there is little temporal variation in the distribution of Y . We also find that Y exhibits temporal independence at all lags, with acf values close to zero (see the Supplementary Material).

We also explore temporal dependence in the covariates. Rohrbeck et al. (2023) states that V_1, \dots, V_4 are temporally independent. We find that for V_6 and V_7 , the acf remains significantly different from zero at all time lags (see the Supplementary Material) due to the changepoint discussed earlier. Finally, V_8 has high acf values at the earliest lags that decrease rapidly until lag 25 (i.e., the length of a month) and then continue to decrease at a slower rate until ~ 50 time lags. This is because atmosphere is recorded monthly.

As noted in Rohrbeck et al. (2023), 11.7% of the observations have at least one possible predictor variable missing completely at random (MCAR). A detailed breakdown of the pattern of missing predictor observations is provided in the Supplementary Material. Since we can assume the data are MCAR, ignoring the observations that have a missing predictor variable will not bias our inference. However, a complete case analysis is undesirable due to the amount of data loss. To mitigate against this, we attempt to impute the observations where predictors are missing but ultimately found a case analysis approach works best for our data. This results in only 4% of observations being removed for our final model.

3.2 Methods

In this section, we explain our model development procedure for $Y \mid \mathbf{X}$. As the challenges concern extreme quantile estimation, we use a non-stationary GPD model. This requires threshold selection and comparison of different covariate-dependent GPD parameterisations. Recall that we utilise the same model formulation for both C1 and C2 via (3.1).

When fitting a GPD, the first challenge is to select an appropriate threshold. This selection involves a bias-variance trade-off: too low a threshold is likely to violate the asymptotic basis of the model, incorporating bias in the GPD fit, whereas higher threshold choices lead to additional uncertainty due to fewer exceedances being used to fit the model. A variety of methods exist which aim to balance this trade-off; Scarrott and MacDonald (2012) provide a review and more recent developments include Northrop et al. (2017) and Schneider et al. (2021). Owing to its favourable properties for IID data, we employ the threshold selection method of Murphy et al. (2023) and extend this approach to select a threshold for non-stationary, covariate-dependent GPD models. The method selects a threshold based on minimising the expected quantile discrepancy (EQD) between the sample quantiles and fitted GPD model quantiles. When fitting a non-stationary model, the excesses will not be identically distributed across covariates. Thus, to utilise the EQD method in this case, we use the fitted non-stationary GPD parameter estimates to transform the excesses to common standard exponential margins and compare sample quantiles against theoretical quantiles from the standard exponential distribution.

Owing to the complex covariate structure observed in the data, as described in Section 3.1, we employ the flexible EVGAM framework proposed in Youngman (2019) for modelling GPD tail behaviour. Under this framework, GAM formulations are used to capture non-stationarity in the threshold, scale and shape functions introduced in Section 2. In general, GAMs provide flexible functional forms that allow us to capture multiple covariate interactions. Moreover, both discrete and continuous covariates can be incorporated in the GAM framework.

Without loss of generality, consider the scale function $\sigma(\mathbf{x})$. We assume that

$$h(\sigma(\mathbf{x})) = \psi_\sigma(\mathbf{x}), \quad \text{with} \quad \psi_\sigma(\mathbf{x}) = \beta_0 + \sum_{\kappa=1}^K \sum_{p=1}^{P_\kappa} \beta_{\kappa p} b_{\kappa p}(\mathbf{x}), \quad (3.3)$$

where $h(x) := \log(x)$ denotes the link function which ensures the correct support, with coefficients $\beta_0, \beta_{\kappa p} \in \mathbb{R}$ and basis functions $b_{\kappa p}$ for $p \in \{1, \dots, P_\kappa\}, \kappa \in \{1, \dots, K\}$. Analogous forms are taken for $v(\mathbf{x})$ and $\xi(\mathbf{x})$, adjusting the link function h as appropriate, with ψ_v and ψ_ξ denoting the respective formulations.

For all GAM formulations, model fitting is carried out using the `evgam` software package (Youngman, 2022), whereby restricted maximum likelihood estimation (REML) is used to approximate the GAM coefficients. In general, REML schemes avoid over-fitting through penalisation of the likelihood function. Furthermore, formulation via likelihood functions avoids the use of Markov Chain Monte-Carlo methods, which can be computationally expensive; see Wood (2017) for further details.

For model performance assessment and selection, we apply k -fold CV (Hastie et al., 2001, Ch 7.). We divide the data into k groups (folds), where each fold is removed in turn and the model is fitted to the remaining data. Choosing a higher number k provides less biased CV metrics with a higher variance. A lower k is computationally cheaper, however, it may overestimate the test error rate. We explore model ranking by taking both $k = 10$ and 50, and find that both give an equivalent ranking; we present results for the latter. For each omitted fold, we compute several goodness-of-fit measures: Akaike Information Criterion (AIC), Bayesian Information Criterion (BIC), and the continuous ranked probability score (CRPS, Gneiting and Katzfuss, 2014). AIC and BIC aid in guiding the model search, favouring parsimony by penalising model complexity, while CRPS describes the discrepancy between the predicted distribution function and observed values without the specification of empirical quantiles. Finally, we report the average criterion over all 50 folds for each model; lower values of AIC, BIC and CRPS indicate a better model fit.

3.2.1 Model selection

Our analysis in Section 3.1 indicates that V_3 , V_5 (season), and V_6 (wind speed) exhibit non-trivial dependence relationships with the response variable; we therefore assume these variables can be used as predictor variables for modelling Y , and set $\tilde{\mathbf{X}} := (\mathbf{V}_j)_{j \in \{3,5,6\}}$, with $\tilde{X}_{r,t}$ denoting the r^{th} component of $\tilde{\mathbf{X}}$, $r \in \{1,2,3\}$. Although V_7 (wind direction) also exhibits predictor power, we have not considered it here since it is highly correlated with wind speed so would involve adding complex interaction terms to the model formulation, and V_6 has a stronger relationship with Y compared to V_7 (see Figure 1).

There is a clear variation in the distribution of Y between seasons. Due to this distinct difference, we explore the inclusion of a stepped-threshold according to season. In particular, we set $v(\tilde{\mathbf{x}}_t) := \mathbb{1}(\tilde{x}_{2,t} = 1)v_1 + \mathbb{1}(\tilde{x}_{2,t} = 2)v_2$, $v_1, v_2 \in \mathbb{R}$, with corresponding rate parameter $\lambda(\tilde{\mathbf{x}}_t) := \mathbb{1}(\tilde{x}_{2,t} = 1)\lambda_1 + \mathbb{1}(\tilde{x}_{2,t} = 2)\lambda_2$, where $\lambda_1, \lambda_2 \in [0, 1]$ denote the non-exceedance probabilities for seasons 1 and 2, respectively. This seasonal threshold significantly improves model fits; see the Supplementary Material for further details. GAM forms for the threshold were also explored, but did not offer significant improvement. Furthermore, the smooth GAM formulation of the GPD scale parameter adequately captures any residual variation in the response arising due to covariate dependence.

Using the `evgam` package, we fit the non-stationary GPD to the tail of Y , with $\sigma(\mathbf{x})$ as in equation (3.3). We keep the shape function $\xi(\mathbf{x}) := \xi \in \mathbb{R}$ constant across covariates; this is common in non-stationary analyses, since this parameter is difficult to estimate (Chavez-Demoulin and Davison, 2005). Even after accounting for seasonal variability in the threshold, including the seasonal variable in the scale function formulation via an indicator function improves model fits. From Section 3.1, we know there is a step change in the mean for V_6 ; we consider both an indicator function and a spline to capture the relationship between Y and this predictor. When using splines, we are required to select a basis dimension $B \in \mathbb{N}$; this determines the number of

coefficients to be estimated. Basis dimension is the most important choice within spline modelling procedures and directly corresponds with the flexibility of the framework (Wood, 2017). In practice, it is better to select a higher dimension than we would expect to be necessary since the REML scheme will adjust estimates of coefficients to avoid over-fitting. Furthermore, as long as the basis dimension is sufficiently high, the locations of knots have little impact on the resulting model fits. Note that we use thin-plate regression splines as they can smooth with respect to any number of covariates, and it is the default in the `evgam` package (Youngman, 2022). Other types of splines could be used, but we do not consider them here.

To determine B for V_6 , we build a model for $Y \mid \tilde{X}_3$, allowing us to consider the effect of this predictor on the response directly. We vary the basis dimension, and compare the resulting models using CV. Through this, we set $B = 3$ since this appears to offer sufficient flexibility to capture the observed dependence. For V_3 , we employ a similar procedure and set $B = 4$.

To determine the best-fitting model, we use a forward selection process based on minimising the CV score using CRPS. Specifically, by comparing model fits with only a single predictor variable (models 2-4 in Table 1), we find model 4 minimises the CV score and so we add V_3 to the model. Continuing in this fashion results in our final model being model 7. Wind speed (V_6) was also modelled using an indicator function to try and capture its changepoint although this did not improve the model fit and has been omitted in Table 1. We have omitted models that included additional predictor variables and interaction terms as they do not reduce the CV score further.

Let y_t and \tilde{x}_t denote the observations of the response variable and predictive covariates, respectively. Then our model has the following form,

$$F_{Y_t|\tilde{X}_t}(y_t|\tilde{X}_t = \tilde{x}_t, y_t > v(\tilde{x}_t)) = 1 - \lambda(\tilde{x}_t) \left[1 + \xi \left(\frac{y_t - v(\tilde{x}_t)}{\sigma(\tilde{x}_t)} \right) \right]_+^{-1/\xi},$$

for all $t \in \{1, \dots, n\}$. The formulation of $\sigma(\cdot)$ is defined in Table 1 as model 7, where $\beta_0, \beta_1 \in \mathbb{R}$ denote coefficients, and s_1, s_2 are thin-plate regression splines for V_3 and V_6 , respectively, with corresponding basis coefficients $\beta_2 \in \mathbb{R}^3$ and $\beta_3 \in \mathbb{R}^4$.

Table 1: Table of selected models considered for challenge C1. $\mathbb{1}(\cdot)$ denotes an indicator function, $s_i(\cdot)$ for $i \in \{1, 2\}$ denote thin-plate regression splines, β_0, β_1 are coefficients to be estimated, and $\tilde{x}_{r,t}$ is defined as in the text. All values have been given to one decimal place.

Model	$\sigma(\tilde{\mathbf{x}}_t)$	CRPS	AIC	BIC
1	β_0	11.5	92,059.9	92,074.5
2	$\beta_0 + \beta_1 \mathbb{1}(\tilde{x}_{2,t} = 1)$	11.0	92,026.5	92,048.4
3	$\beta_0 + s_1(\tilde{x}_{1,t})$	10.6	91,651.4	91,695.3
4	$\beta_0 + s_2(\tilde{x}_{3,t})$	11.0	91,775.6	91,797.7
5	$\beta_0 + \beta_1 \mathbb{1}(\tilde{x}_{2,t} = 1) + s_1(\tilde{x}_{1,t})$	10.6	91,634.1	91,686.4
6	$\beta_0 + s_1(\tilde{x}_{1,t}) + s_2(\tilde{x}_{3,t})$	10.5	91,307.2	91,357.3
7	$\beta_0 + \beta_1 \mathbb{1}(\tilde{x}_{2,t} = 1) + s_1(\tilde{x}_{1,t}) + s_2(\tilde{x}_{3,t})$	10.4	91,279.9	91,339.2

For challenge C2, we are required to incorporate the loss function of equation (3.2) into the modelling framework. Letting $\mathcal{J}_v := \{t \in \{1, \dots, n\} \mid y_t > v(\tilde{\mathbf{x}}_t)\}$ and $n_v := |\mathcal{J}_v|$, we consider the following objective function

$$S(\boldsymbol{\theta}) := -l_R(\boldsymbol{\theta}) + \sum_{i \in \mathcal{J}_v} \mathcal{L}(q_i^*, \hat{q}_i)/n_v,$$

where $l_R(\boldsymbol{\theta})$ denotes the penalised log-likelihood function of the REML approach (Wood, 2017), $\boldsymbol{\theta} := (\beta_0, \beta_1, \beta_2, \beta_3, \xi)$ denotes the parameter vector associated with the GPD formulation, and $\sum_{i \in \mathcal{J}_v} \mathcal{L}(q_i^*, \hat{q}_i)/n_v$ denotes the average loss between observed and model quantiles. Specifically, if we denote the mapping between \mathcal{J}_v and the order statistics of $(y_t - v(\tilde{\mathbf{x}}_t))_{t \in \mathcal{J}_v}$ by π , then q_i^* is the $\pi(i)^{\text{th}}$ order statistic of $(y_t - v(\tilde{\mathbf{x}}_t))_{t \in \mathcal{J}_v}$ and $\hat{q}_i = \sigma(\mathbf{x}_{\pi(i)})[\{1 - \pi(i)/(n_v + 1)\}^{-\xi} - 1]/\xi$. Minimising $S(\boldsymbol{\theta})$ ensures the parameter estimates also account for the loss function. We use this formulation to adjust the GPD parameters for challenge C2 once a threshold is selected.

3.3 Uncertainty quantification

We are required to construct central 50% confidence intervals for 100 different covariate combinations provided by the challenge organisers, \mathbf{x}_i for $i \in \{1, \dots, 100\}$. We approximate these intervals using the stationary bootstrapping procedure adopted by D’Arcy et al. (2023) that preserves temporal dependence and covariate information; we outline this below.

First, the response variable Y_t is transformed to Uniform(0,1) margins; denote this sequence $U_t^Y = F_{Y_t|\tilde{\mathbf{X}}_t}(Y_t|\tilde{\mathbf{X}}_t = \tilde{x}_t)$. We then adopt the stationary bootstrap procedure of Politis and Romano (1994) to retain the temporal dependence in the response and explanatory variables. The block length L is simulated from a Geometric($1/l$) distribution, where the mean block length $l \in \mathbb{N}$ is carefully selected based on the autocorrelation function. This was selected at 50 days; the maximum lag for which the autocorrelation was significant across all variables; see the Supplementary Material. Denote this bootstrapped sequence on Uniform margins by U_t^B . We transform U_t^B back to the original scale using our fitted model, preserving the original structure of Y_t ; we denote this series Y_t^B . Then we fit our model to Y_t^B to re-estimate all of the parameters and thus the quantile of interest. We repeat this procedure to obtain 200 bootstrap samples.

3.4 Results

For C1, we use our final model of Section 3.2 to estimate the 0.9999-quantile of $Y | \tilde{\mathbf{X}} = \tilde{x}_i$, $i \in \{1, \dots, 100\}$, for the set of 100 covariate combinations. The left panel of Figure 2 shows the quantile-quantile (QQ) plot for our model. There is general alignment between the model and empirical quantiles; however, there is some under-estimation in the upper tail, and our 95% tolerance bounds do not contain some of the most extreme response values. The right panel of Figure 2 shows our predicted quantiles, and their association confidence intervals, compared to their true quantiles. This figure is different from the one presented by Rohrbeck et al. (2023) due to an error in our code being fixed after submission. In this scenario, our estimated confidence intervals lead to a 14% coverage of the true quantiles, which does not alter our ranking for this challenge. Our performance and model improvements are discussed in Section 6.

For challenge C2, we estimate the quantile of interest as $\hat{q} = 212.5913$ (208.3783, 246.0764). Due to a coding error, this value differs from the original estimate submitted for the data challenge. The updated estimate over-estimates compared to the truth. A 95% confidence interval for the estimate is given in parentheses based on the bootstrapping procedure outlined in Section 3.3.

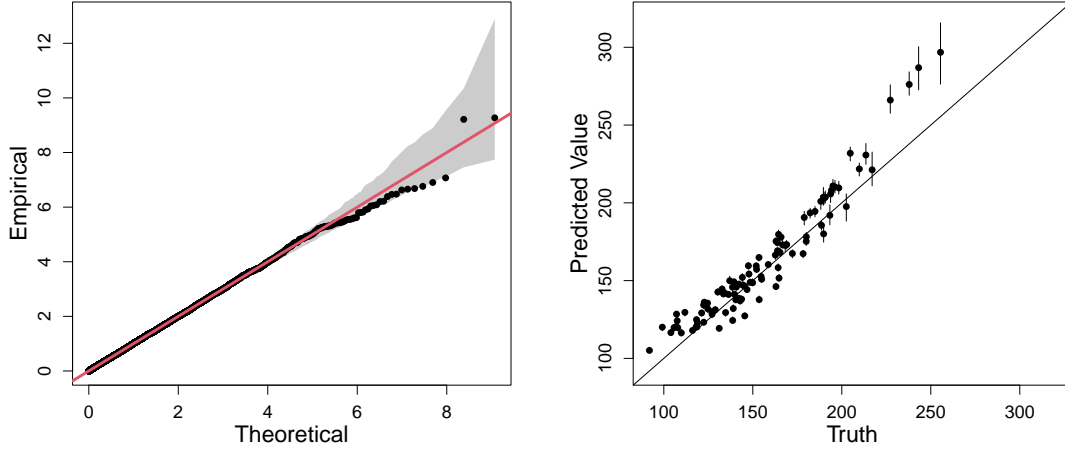


Figure 2: QQ plot for our final model, model 7 in Table 1, on exponential margins. The $y = x$ line is given in red and the grey region represents the 95% tolerance bounds (left). Predicted 0.9999–quantiles against true quantiles for the 100 covariate combinations. The points are the median predicted quantile over 200 bootstrapped samples and the vertical error bars are the corresponding 50% confidence intervals. The $y = x$ line is also shown (right).

4 Challenge C3

4.1 Exploratory data analysis

For challenge C3, we are provided with 70 years of daily time series of an environmental variable for three towns on the island of Coputopia. These series are denoted by $Y_{i,t}$, $i \in \{1, 2, 3\}$, $t \in \{1, \dots, n\}$, where i is the index of each town and t is the point in time. Each year consists of 12 months, each lasting 25 days, resulting in $n = 21,000$ observations for each location.

Alongside the time series, we are also provided with daily covariate observations $\mathbf{X}_t = (S_t, A_t)$, where S_t and A_t denote seasonal and atmospheric conditions, respectively. Season is a binary variable, taking values in the set $\{1, 2\}$, with each year of observations exhibiting both seasons for exactly 150 consecutive days. On the other hand, the atmospheric conditions are piecewise constant over months, with large variation in the observed values between months. A descriptive figure of both covariates is given in the Supplementary Material.

In Rohrbeck et al. (2023), we are informed that $Y_{i,t}$ are distributed identically across all sites and over time, with a standard Gumbel distribution function. However, it is not known whether the covariates \mathbf{X}_t influence the dependence structure of $\mathbf{Y}_t := (Y_{1,t}, Y_{2,t}, Y_{3,t})$. We are also informed that, conditioned on covariates, the process is independent over time, i.e., $(\mathbf{Y}_t | \mathbf{X}_t) \perp\!\!\!\perp (\mathbf{Y}_{t'} | \mathbf{X}_{t'})$ for any $t \neq t'$. In this section, we examine what influence, if any, the covariate process \mathbf{X}_t may have on the dependence structure of \mathbf{Y}_t . If such relationships exist, they need to be accounted for when estimating joint tail probabilities.

We begin by transforming the time series to standard exponential margins using the probability integral transform, i.e., set $Z_{i,t} := -\log(1 - F(Y_{i,t}))$, $i \in \{1, 2, 3\}$, $t \in \{1, \dots, n\}$, where $F(y) = \exp(-\exp(-y))$, $y \in \mathbb{R}$. This transformation is common in the study of multivariate extremes and can simplify the description of extremal dependence (Keef et al., 2013). To explore the extremal dependence in the Coputopia time series, we consider all 2- and 3-dimensional subvectors of the process, i.e., $\{Z_{i,t}, i \in I, t \in \{1, \dots, n\}\}$, $I \in \mathcal{I} := \{\{1, 2\}, \{1, 3\}, \{2, 3\}, \{1, 2, 3\}\}$. This separation is important to ensure the overall dependence structure is fully understood, since intermediate scenarios can exist where a random vector exhibits $\chi = 0$, but $\chi > 0$ for some 2-dimensional subvector(s) (Simpson et al., 2020).

Furthermore, to explore the impact of covariates on the dependence structure, we partition the time series into subsets using the covariates. For the seasonal covariate, let $G_{I,j}^S := \{Z_{i,t}, i \in I, S_t = j\}$ for $j = 1, 2$. For the atmospheric covariate, we let $\pi : \{1, \dots, n\} \rightarrow \{1, \dots, n\}$ denote the permutation associated with the order statistics of A_t , defined so that ties in the data are accounted for. We then split the data into 10 equally sized subsets corresponding to the atmospheric order statistics, i.e., $G_{I,k}^A := \{Z_{i,t}, i \in I, t \in \Sigma^k\}$ for $k = 1, 2, \dots, 10$, where $\Sigma^k := \{t \mid (k-1)n/10 + 1 \leq \pi(t) \leq kn/10\}$. We can observe that the atmospheric values associated with each subset $G_{I,k}^A$ will increase over k .

The idea behind these subsets is to examine whether altering the values of either covariate impacts the extremal dependence structure. Consequently, we set $u = 0.9$ and estimate $\chi(u)$ using

the techniques outlined in Section 2, with uncertainty quantified through bootstrapping with 200 samples. The bootstrapped χ estimates for $G_{I,k}^A$ with $I = \{1, 2, 3\}$ are given in Figure 3. The plots for the remaining index sets in \mathcal{I} , along with the subsets associated with the seasonal covariate, are given in the Supplementary Material. The estimates of χ appear to vary, in the majority of cases, across both subset types (seasonal and atmospheric), suggesting both covariates have an impact on the dependence structure. For the atmospheric process in particular, the values of χ tend to decrease for higher atmospheric values, suggesting a negative association between positive extremal dependence and atmosphere. We also observe that across all subsets, χ appears consistently low in magnitude, suggesting the extremes of some, if not all, of the sub-vectors are unlikely to occur simultaneously. As such, for modelling the Coputopia time series, we require a framework that can capture such forms of dependence.

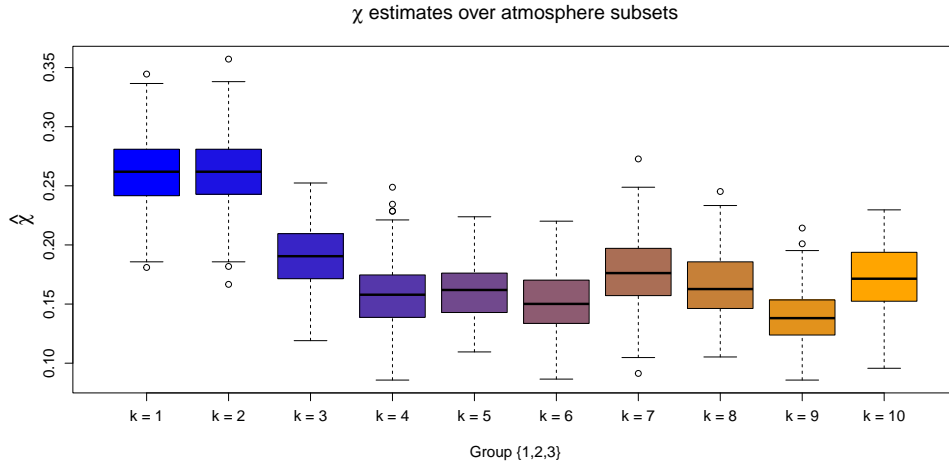


Figure 3: Boxplots of empirical χ estimates obtained for the subsets $G_{I,k}^A$, with $k = 1, \dots, 10$ and $I = \{1, 2, 3\}$. The colour transition (from blue to orange) over k illustrates the trend in χ estimates as the atmospheric values are increased.

We also consider pointwise estimates of the function λ , as defined later in equation (4.2), over $G_{I,j}^S$ and $G_{I,k}^A$ for fixed simplex points; these results are given in the Supplementary Material. Similar to χ , estimates of λ vary significantly across subsets, providing additional evidence of non-stationarity within extremal dependence structure.

4.2 Modelling of joint tail probabilities under asymptotic independence

For challenge C3, we are required to estimate probabilities $p_1 := \Pr(Y_1 > y, Y_2 > y, Y_3 > y)$ and $p_2 := \Pr(Y_1 > v, Y_2 > v, Y_3 < m)$, with $y = 6$, $v = 7$ and $m = -\log(\log(2))$. We refer to p_1 and p_2 as parts 1 and 2 of the challenge, respectively. Note that p_1 and p_2 are independent of the covariate process and correspond to different extremal regions in \mathbb{R}^3 . For the remainder of this section we will consider the transformed exponential variables (Z_1, Z_2, Z_3) , omitting the subscript t for ease of notation. Observe that $F_{(-Z_3)}(z) = e^z$, for $z < 0$; setting $\tilde{Z}_3 := -\log(1 - \exp\{-Z_3\})$, we have

$$p_2 = \Pr(Z_1 > \tilde{v}, Z_2 > \tilde{v}, Z_3 < \tilde{m}) = \Pr(Z_1 > \tilde{v}, Z_2 > \tilde{v}, \tilde{Z}_3 > \tilde{m}),$$

where \tilde{v} and \tilde{m} denote the values v and m transformed to the standard exponential scale, e.g., $\tilde{v} := -\log(1 - \exp\{-\exp\{-v\}\})$. Similarly, we have $p_1 = \Pr(Z_1 > \tilde{y}, Z_2 > \tilde{y}, Z_3 > \tilde{y})$. Consequently, both p_1 and p_2 can be considered as joint survivor probabilities.

In many applications of multivariate extremes, joint tail probabilities are estimated using models that implicitly assume random vectors are regularly varying (Tawn, 1988; Resnick, 2002). However, this framework is unable to accurately extrapolate into the joint tail for data not exhibiting asymptotic dependence (Ledford and Tawn, 1996; Heffernan and Tawn, 2004). This has motivated the development of modelling approaches for data structures where not all extremes are observed simultaneously, such as the Coputopia data set.

The first such approach was proposed by Ledford and Tawn (1996); given a slowly varying function \mathcal{L} , i.e., $\lim_{u \rightarrow 1} \mathcal{L}(tu)/\mathcal{L}(u) = 1$ for all $t > 0$, they assume the joint tail is given by

$$\Pr(Z_1 > u, Z_2 > u, Z_3 > u) = \Pr(\min\{Z_1, Z_2, Z_3\}) = \mathcal{L}(e^u) e^{-u/\eta}, \quad (4.1)$$

as $u \rightarrow \infty$, where $\eta \in (0, 1]$ is the coefficient of tail dependence defined in Section 2. If $\eta = 1$ and $\lim_{u \rightarrow \infty} \mathcal{L}(u) \neq 0$, we have asymptotic dependence, while $\eta < 1$, or $\eta = 1$ and $\lim_{u \rightarrow \infty} \mathcal{L}(u) = 0$, implies the variables cannot be extreme simultaneously.

In practice, the approach of Ledford and Tawn (1996) is only applicable within regions where

all variables are large. To overcome this limitation, Wadsworth and Tawn (2013) proposed a general extension of equation (4.1). For any ray $\omega \in \mathcal{S}^2 := \{(w_1, w_2, w_3) \in [0, 1]^3 : w_1 + w_2 + w_3 = 1\}$, where \mathcal{S}^2 denotes the standard 2-dimensional simplex, the authors assume

$$\begin{aligned} \Pr(Z_1/w_1 > r, Z_2/w_2 > r, Z_3/w_3 > r) &= \Pr(\min\{Z_1/w_1, Z_2/w_2, Z_3/w_3\} > r) \\ &= \mathcal{L}(e^r; \omega) e^{-r\lambda(\omega)}, \end{aligned} \quad (4.2)$$

as $r \rightarrow \infty$, where $\lambda(\omega) \geq \max(\omega)$ is known as the angular dependence function. Asymptotic dependence occurs at the lower bound, i.e., $\lambda(\omega) = \max(\omega)$ for all $\omega \in \mathcal{S}^2$, and model (4.2) reduces to model (4.1) for $\omega = (1/3, 1/3, 1/3)$, with $\eta = 1/\{3\lambda(\omega)\}$. In practice, equation (4.2) can be used to evaluate extreme joint survivor probabilities; in particular, probabilities p_1 and p_2 can be identified with the rays $\omega^{(1)} := (\tilde{u}, \tilde{u}, \tilde{u})/r^{(1)}$ and $\omega^{(2)} := (\tilde{v}, \tilde{v}, \tilde{m})/r^{(2)}$ in \mathcal{S}^2 , respectively, where $r^{(1)} := \tilde{u} + \tilde{u} + \tilde{u}$ and $r^{(2)} := \tilde{v} + \tilde{v} + \tilde{m}$. See Section 4.4 for further details.

As a final remark, we note that there exist several additional methods capable of approximating extreme joint survivor probabilities for non-asymptotically dependent data structures (e.g., Heffernan and Tawn, 2004; Wadsworth et al., 2017). However, in our approach, we prefer to stick with the model of Wadsworth and Tawn (2013) since this framework can be easily adapted to capture non-stationary dependence.

4.3 Accounting for non-stationary dependence

In the stationary setting, pointwise estimates of λ can be obtained via the Hill estimator (Hill, 1975), from which tail probabilities can be approximated. However, alternative procedures are required for data exhibiting trends in dependence, such as the Coputopia data set. Existing approaches for capturing non-stationary dependence structures are sparse in the extremes literature, and most approaches are limited to asymptotically dependent data structures. For the case when data are not asymptotically dependent, Mhalla et al. (2019) and Murphy-Barltrop and Wadsworth (2022) propose non-stationary extensions of the Wadsworth and Tawn (2013) framework, while Jonathan et al. (2014) and Guerrero et al. (2023) propose non-stationary extensions of the Heffer-

nan and Tawn (2004) model. See Murphy-Barltrop and Wadsworth (2022) for a detailed review.

To account for non-stationary dependence in C3, we propose an extension of the Wadsworth and Tawn (2013) framework. With $\mathbf{Z}_t = (Z_{1,t}, Z_{2,t}, Z_{3,t})$ and \mathbf{X}_t , defined as in Section 4.1, we define the structure variable $T_{\omega,t} := \min\{Z_{1,t}/w_1, Z_{2,t}/w_2, Z_{3,t}/w_3\}$, for any $\omega \in \mathcal{S}^2$; we refer to $T_{\omega,t}$ as the min-projection at time t . From Section 4.1, we know that the joint distribution of \mathbf{Z}_t is not identically distributed over t ; this implies non-stationarity in the distribution of $T_{\omega,t}$.

To account for non-stationarity in $T_{\omega,t}$, Mhalla et al. (2019) and Murphy-Barltrop and Wadsworth (2022) assume the following model

$$\Pr(T_{\omega,t} > u \mid \mathbf{X}_t = \mathbf{x}_t) = \mathcal{L}(e^u \mid \omega, \mathbf{x}_t) e^{-\lambda(\omega \mid \mathbf{x}_t)u} \text{ as } u \rightarrow \infty, \quad (4.3)$$

for all t . Note that this assumption is very similar in form to equation (4.2), with the primary difference being the function λ is non-stationary over t . From equation (4.3), it is straightforward to see that

$$\Pr(T_{\omega,t} - u > z \mid T_{\omega,t} > u, \mathbf{X}_t = \mathbf{x}_t) = e^{-\lambda(\omega \mid \mathbf{x}_t)z} \text{ as } u \rightarrow \infty, \quad (4.4)$$

for $z > 0$. Consequently, equation (4.3) is equivalent to assuming $(T_{\omega,t} - u) \mid \{T_{\omega,t} > u, \mathbf{X}_t = \mathbf{x}_t\} \sim \text{Exp}(\lambda(\omega \mid \mathbf{x}_t))$ as $u \rightarrow \infty$.

In unreported exploratory analysis, we found that equation (4.3) was not flexible enough to capture the tail of $T_{\omega,t}$ for the Coputopia data; see section 4.3.2 for further discussion. Thus, we propose the following model: given any $z > 0$ and a fixed $\omega \in \mathcal{S}^2$, we assume

$$\Pr(T_{\omega,t} - u > z \mid T_{\omega,t} > u, \mathbf{X}_t = \mathbf{x}_t) = \left(1 + \frac{\xi(\omega \mid \mathbf{x}_t)z}{\sigma(\omega \mid \mathbf{x}_t)}\right)^{-1/\xi(\omega \mid \mathbf{x}_t)} \text{ as } u \rightarrow \infty. \quad (4.5)$$

This is equivalent to assuming $(T_{\omega,t} - u) \mid \{T_{\omega,t} > u, \mathbf{X}_t = \mathbf{x}_t\} \sim \text{GPD}(\sigma(\omega \mid \mathbf{x}_t), \xi(\omega \mid \mathbf{x}_t))$ as $u \rightarrow \infty$, and equation (4.4) is recovered by taking the limit as $\xi(\omega \mid \mathbf{x}_t) \rightarrow 0$ for all t .

Our proposed formulation in equation (4.5) allows for additional flexibility within the modelling framework via the inclusion of a GPD shape parameter $\xi(\omega \mid \mathbf{x}_t)$, which quantifies the tail behaviour of $T_{\omega,t}$. Given the wide range of distributions in the domain of attraction of a GPD

(Pickands, 1975), it is reasonable to assume that the tail of $T_{\omega,t}$ can be approximated by equation (4.5). For the Coputopia time series, this assumption appears valid, as demonstrated by the diagnostics in Section 4.3.2.

4.3.1 Model fitting

To apply equation (4.5), we first fix $\omega \in \mathcal{S}^2$ and assume that the formulation holds approximately for some sufficiently high threshold level from the distribution of $T_{\omega,t}$; we denote the corresponding quantile level by $\tau \in (0, 1)$. For simplicity, the same quantile level is considered across all t . Further, let $v_\tau(\omega, \mathbf{x}_t)$ denote the corresponding threshold function, i.e., $\Pr(T_{\omega,t} \leq v_\tau(\omega, \mathbf{x}_t) \mid \mathbf{X}_t = \mathbf{x}_t) = \tau$ for all t . Under our assumption, we have $(T_{\omega,t} - v_\tau(\omega, \mathbf{x}_t)) \mid \{T_{\omega,t} > v_\tau(\omega, \mathbf{x}_t), \mathbf{X}_t = \mathbf{x}_t\} \sim \text{GPD}(\sigma(\omega \mid \mathbf{x}_t), \xi(\omega \mid \mathbf{x}_t))$. We emphasise that $v_\tau(\omega, \mathbf{x}_t)$ is not constant in t , and we would generally expect $v_\tau(\omega, \mathbf{x}_t) \neq v_\tau(\omega, \mathbf{x}_{t'})$ for $t \neq t'$.

As detailed in Section 4.2, both p_1 and p_2 can be associated with points on the simplex \mathcal{S}^2 , denoted by $\omega^{(1)}$ and $\omega^{(2)}$, respectively. Letting $\omega \in \{\omega^{(1)}, \omega^{(2)}\}$, our estimation procedure consists of two stages: estimation of threshold function $v_\tau(\omega, \mathbf{z}_t)$ for a fixed $\tau \in (0, 1)$, followed by estimation of GPD parameter functions $\sigma(\omega \mid \mathbf{x}_t), \xi(\omega \mid \mathbf{x}_t)$. For both steps, we take a similar approach to Section 3.2 and use GAMs to capture these covariate relationships. To simplify our approach, we falsely assume that the atmospheric covariate A_t is continuous over t ; this step allows us to utilise GAM formulations containing smooth basis functions. Given the significant variability in A_t between months, discrete formulations for this covariate would significantly increase the number of model parameters and result in higher variability.

Let $\log(v_\tau(\omega, \mathbf{x}_t)) = \psi_v(\mathbf{x}_t)$, $\log(\sigma(\omega \mid \mathbf{x}_t)) = \psi_\sigma(\mathbf{x}_t)$ and $\xi(\omega \mid \mathbf{x}_t) = \psi_\xi(\mathbf{x}_t)$ denote the GAM formulations of each function, where ψ_- denotes the basis representation of equation (3.3). Exact forms of basis functions are specified in Section 4.3.2. As in Section 3.2, model fitting is carried out using the `evgam` software package (Youngman, 2022), with REML procedures used to avoid over-fitting. For the first stage, $v_\tau(\omega, \mathbf{x}_t)$ is estimated by exploiting a link between the loss

function typically used for quantile regression and the asymmetric Laplace distribution (Yu and Moyeed, 2001). The spline coefficients associated with ψ_σ and ψ_ξ are estimated subsequently using the obtained threshold exceedances.

4.3.2 Selection of GAM formulations and diagnostics

Prior to estimation of the threshold and parameter functions, we specify a quantile level τ and formulations for each of the GAMs. To begin, we fix $\tau = 0.9$ and restrict attention to the latter problem; this in turn involves selecting basis functions and basis dimensions. A variety of formulations were considered for each GAM. By comparing metrics for model selection, namely AIC, BIC and CRPS, we found the following formulations to be sufficient

$$\psi_v(x_t) = \beta_u + s_v(a_t) + \beta_s \mathbb{1}(s_t = 2), \quad \psi_\sigma(x_t) = \beta_\sigma + s_\sigma(a_t) \quad \text{and} \quad \psi_\xi(x_t) = \beta_\xi, \quad (4.6)$$

for parts 1 and 2, where $\beta_u, \beta_\sigma, \beta_\xi \in \mathbb{R}$ denote constant intercept terms, $\mathbb{1}$ denotes the indicator function with corresponding coefficient $\beta_s \in \mathbb{R}$, and s_u, s_σ denote cubic regression splines of dimension $B = 10$. The shape parameter is set to constant for the reasons outlined in Section 3.2.1. Cubic basis functions are used for ψ_v and ψ_σ since they have several desirable properties, including continuity and smoothness (Wood, 2017). Setting $B = 10$ appears more than sufficient to capture the trends relating to the atmosphere variable. Alternative smooth splines and basis dimensions were tested for both parts 1 and 2, but this made little difference to the resulting model fits. Moreover, the fact the same model selection appeared suitable for both parts of C3 provides evidence of robustness for these GAM formulations.

We remark that the seasonal covariate is only present with the formulation for ψ_v . Once accounted for in the non-stationary threshold, the seasonal covariate appeared to have little influence on the fitted GPD parameters. More complex GAM formulations were tested involving interaction terms between the seasonal and atmospheric covariates. However, such formulations offered negligible improvements in model fits, and thus we prefer the simpler formulations on the basis of parsimony.

With GAM formulations selected, we now consider the quantile level $\tau \in (0, 1)$; this is analogous to the bias-variance trade-off discussed in Section 3.2. To assess sensitivity in our formulation, we set $T := \{0.8, 0.81, \dots, 0.99\}$ and fit the GAMs outlined in equation (4.6) for each $\tau \in T$. Letting $\delta_{\omega,t}$ and $\mathcal{T}_\tau := \{t \in \{1, \dots, n\} \mid \delta_{\omega,t} > v_\tau(\omega, x_t)\}$ denote the min-projection observations and indices of threshold-exceeding observations, respectively, we expect the set $\mathcal{E} := \{-\log\{1 - F_{GPD}(\delta_{\omega,t} - v_\tau(\omega, x_t) \mid \sigma(\omega \mid x_t), \xi(\omega \mid x_t))\} \mid t \in \mathcal{T}_\tau\}$ to be distributed according to a unit exponential distribution.

With all exceedances transformed to a unified scale, we compare the empirical and model exponential quantiles using QQ plots, through which we assess the relative performance of each $\tau \in T$. We then selected τ values for which the empirical and theoretical quantiles appeared most similar in magnitude. From this analysis, we set $\tau = 0.83$ and $\tau = 0.85$ for parts 1 and 2, respectively. The corresponding QQ plots are given in Figure 4, where we observe reasonable agreement between the empirical and theoretical quantiles. However, whilst these values appeared optimal within T , we stress that adequate model fits were also obtained for other quantile levels, suggesting our modelling procedure is not especially sensitive to the exact choice of quantile. Furthermore, we also tested a range of quantile levels below the 0.8-level, but were unable to improve the quality of model fits.

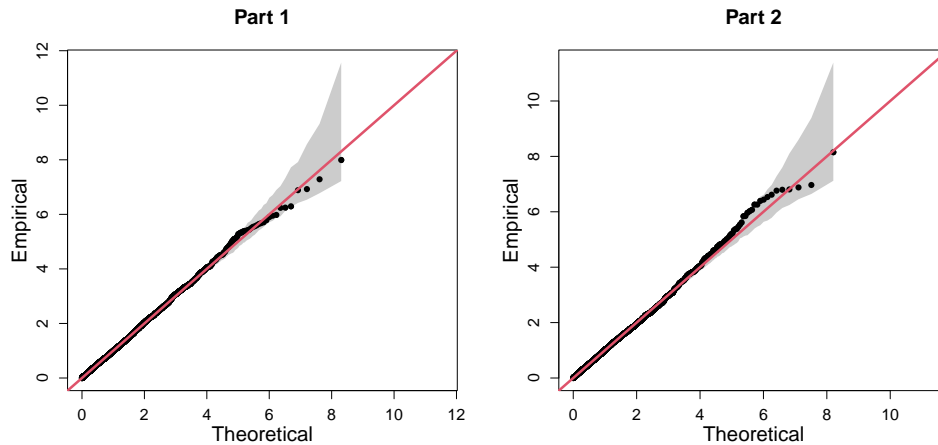


Figure 4: Final QQ plots for parts 1 (left) and 2 (right) of C3, with the $y = x$ line given in red. In both cases, the grey regions represent the 95% bootstrapped tolerance bounds.

Plots illustrating the estimated GPD scale parameter functions are given in the Supplementary Material, with the resulting dependence trends in agreement with the observed trends from Section 4.1. We also remark that the estimated GPD shape parameters obtained for parts 1 and 2 were 0.042 (0.01, 0.075) and 0.094 (0.059, 0.128), respectively, where the brackets denote 95% confidence intervals obtained using posterior sampling; see Wood (2017). These estimates, which indicate slightly heavy-tailed behaviour within the min-projection variable, provide insight into why the original exponential modelling framework is not appropriate for C3.

Overall, these results suggest different extremal dependence trends exist for the two simplex points $\omega^{(1)}$ and $\omega^{(2)}$, illustrating the importance of the flexibility in our model. These findings are also in agreement with empirical trends observed in Section 4.1, suggesting our modelling framework is successfully capturing the underlying extremal dependence structures.

4.4 Results

Given estimates of threshold and parameter functions, probability estimates can be obtained via Monte Carlo techniques. Taking p_1 , for instance, we have

$$\begin{aligned}
p_1 &= \Pr(Z_1 > \tilde{y}, Z_2 > \tilde{y}, Z_3 > \tilde{y}) \\
&= \Pr\left(\min\left(Z_1/w_1^{(1)}, Z_2/w_2^{(1)}, Z_3/w_3^{(1)}\right) > r^{(1)}\right) \\
&= \int_{\mathbf{X}_t} \Pr(T_{\omega^{(1)}, t} > r^{(1)} \mid \mathbf{X}_t = \mathbf{x}_t) f_{\mathbf{X}_t}(\mathbf{x}_t) d\mathbf{x}_t \\
&= (1 - \tau) \int_{\mathbf{X}_t} \Pr(T_{\omega^{(1)}, t} > r^{(1)} \mid T_{\omega^{(1)}, t} > v_\tau(\omega^{(1)}, \mathbf{x}_t), \mathbf{X}_t = \mathbf{x}_t) f_{\mathbf{X}_t}(\mathbf{x}_t) d\mathbf{x}_t \\
&\approx \frac{1 - \tau}{n} \sum_{t=1}^n \left(1 + \frac{\xi(\omega^{(1)} \mid \mathbf{x}_t) (r^{(1)} - v_\tau(\omega^{(1)}, \mathbf{x}_t))}{\sigma(\omega^{(1)} \mid \mathbf{x}_t)} \right)^{-1/\xi(\omega^{(1)} \mid \mathbf{x}_t)},
\end{aligned}$$

assuming $\{\mathbf{x}_t : t \in \{1, \dots, n\}\}$ is a representative sample from \mathbf{X}_t . The procedure for p_2 is analogous. We note that this estimation procedure is only valid when $r^{(1)} > v_\tau(\omega^{(1)}, \mathbf{x}_t)$, or $r^{(2)} > v_\tau(\omega^{(2)}, \mathbf{x}_t)$, for all t : however, for each $\tau \in \mathbf{T}$, this inequality is always satisfied, owing to the very extreme nature of the probabilities in question. Through this approximation, we obtain $\hat{p}_1 = 1.480449 \times 10^{-5}$ and $\hat{p}_2 = 2.460666 \times 10^{-5}$.

5 Challenge C4

5.1 Exploratory data analysis

Challenge C4 entails estimating survival probabilities across 50 locations on the island of Utopula. As stated in Rohrbeck et al. (2023), the Utopula island is split in two administrative areas, for which the respective regional governments 1 and 2 have collected data concerning the variables $Y_{i,t}$, $i \in I = \{1, \dots, 50\}$, $t \in \{1, \dots, 10,000\}$. The index i denotes the i^{th} location, with locations $i \in \{1, \dots, 25\}$ and $i \in \{26, \dots, 50\}$ belonging to the administrative areas of governments 1 and 2, respectively. Index t denotes the time point in days; however, since $Y_{i,t}$ are IID for all i , we drop the subscript t for the remainder of this section.

Many multivariate extreme value models are only applicable in low-to-moderate dimensions, and we would not generally expect such techniques to scale to the 50-dimensional setting (Engelke and Ivanovs, 2021). It is therefore reasonable to consider techniques for dimensional reduction. We explore this possibility by examining the extremal dependence structure of the data. In particular, we look at pairwise $\chi(u)$ extremal dependence coefficients, introduced in equation (2.1), for all possible pairwise combinations of sites; the resulting estimates with $u = 0.95$ are visualised in the heat map of Figure 5.

Figure 5 suggests the existence of 5 distinct subgroups where all variables within each subgroup have similar extremal dependence characteristics, but variables in different subgroups appear to be approximately independent of each other in the extremes. It is worth noting that the same clusters are identified when examining pairwise $\eta(u)$ extremal dependence coefficients; the resulting estimates can be found in the Supplementary Material. Moreover, examining the magnitudes of the aforementioned $\chi(\cdot)$ and $\eta(\cdot)$ estimates, assuming asymptotic dependence between variables in each group does not appear reasonable. We therefore consider models that can be applied to data structures that do not take their extreme values simultaneously. The indices of the five aforementioned subgroups are given by:

$$G_1 = \{4, 14, 19, 28, 30, 38, 43, 44\},$$

$$G_2 = \{3, 10, 15, 18, 22, 29, 45, 47\},$$

$$G_3 = \{8, 21, 25, 26, 32, 33, 34, 40, 41, 42, 48, 49, 50\},$$

$$G_4 = \{1, 2, 5, 7, 9, 17, 20, 31, 46\},$$

$$G_5 = \{6, 11, 12, 13, 16, 23, 24, 27, 35, 36, 37, 39\}.$$

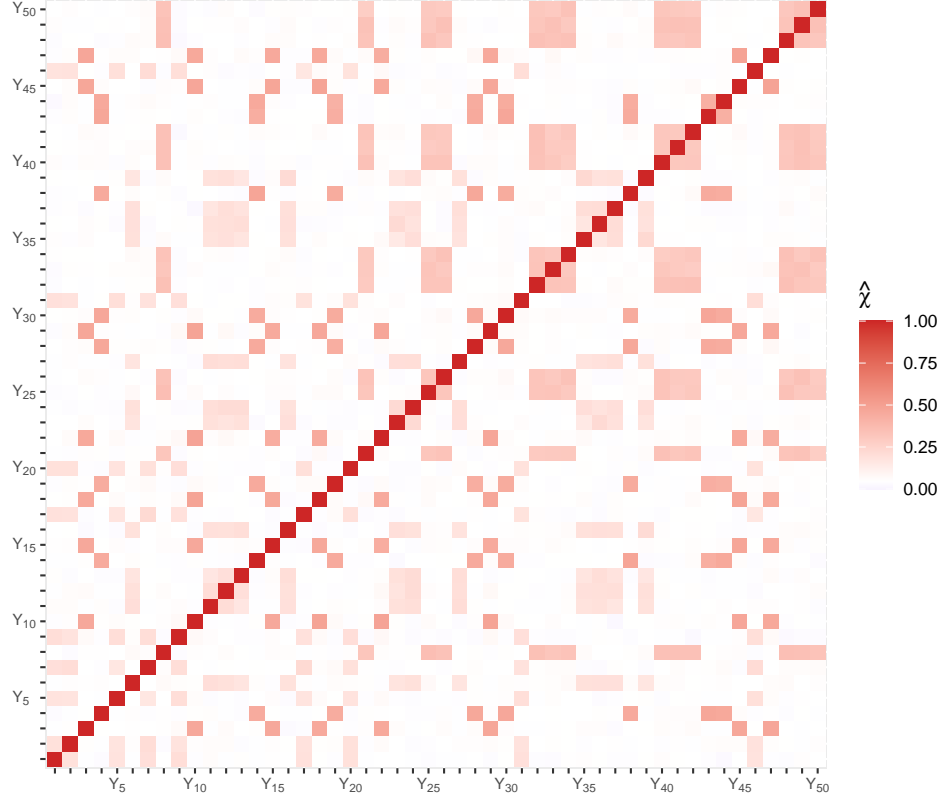


Figure 5: Heat map of estimated empirical pairwise $\chi(u)$ extremal dependence coefficients with $u = 0.95$.

Groups G_1 and G_2 include the most strongly dependent variables (shown by the darkest color blocks in Figure 5), followed by groups G_3 and G_4 , while group G_5 contains the most weakly dependent variables. We henceforth assume independence between these groups of variables, i.e., $\Pr((Y_i)_{i \in G_k} \in A_k, (Y_i)_{i \in G_{k'}} \in A_{k'}) = \Pr((Y_i)_{i \in G_k} \in A_k) \Pr((Y_i)_{i \in G_{k'}} \in A_{k'})$, $A_k \subset \mathbb{R}^{|G_k|}, A_{k'} \subset \mathbb{R}^{|G_{k'}|}$, for any $k \neq k' \in \{1, \dots, 5\}$.

Challenge C4 requires us to estimate the probabilities $p_1 = \Pr(Y_i > s_i; i \in I)$ and $p_2 = \Pr(Y_i >$

$s_1; i \in I$), where $s_i := \mathbb{1}(i \in \{1, 2, \dots, 25\})s_1 + \mathbb{1}(i \in \{26, 27, \dots, 50\})s_2$ and s_1 (s_2) denotes the marginal level exceeded once every year (month) on average. We refer to p_1 and p_2 as parts 1 and 2 of C4, respectively. Under the assumption of independence between groups, the challenge can be broken down to 5 lower-dimensional challenges involving the estimation of joint tail probabilities for each G_k , $k \in \{1, \dots, 5\}$. These can then be multiplied together to obtain the required overall probabilities due to (assumed) between-group independence. Specifically, we have $p_1 = \prod_{k=1}^5 \Pr(Y_i > s_i; i \in G_k)$ and $p_2 = \prod_{k=1}^5 \Pr(Y_i > s_1; i \in G_k)$. We now consider estimation of within group probabilities.

5.2 Conditional extremes

In this section, we detail the modelling approach proposed by Heffernan and Tawn (2004), commonly referred to as the conditional extremes model. The main appeal of this approach is that it provides a flexible multivariate extreme value framework, capable of capturing a range of extremal dependence forms. It has thus been applied extensively to the joint modelling of environmental data sets (Keef et al., 2013; Jonathan et al., 2014) and in the high dimensional setting (e.g., Quinn et al., 2019). For these reasons, we opt to employ this as our method for modelling extremes in challenge C4.

Consider a d -dimensional random variable $\mathbf{W} = (W_1, \dots, W_d)$ on Laplace margins. The conditional extremes model approach assumes the existence of normalising functions $\mathbf{a}_{|i}$, $\mathbf{b}_{|i}$ such that

$$\lim_{w_i \rightarrow \infty} \Pr \{ \mathbf{W}_{-i} \leq \mathbf{a}_{|i}(w_i) + \mathbf{b}_{|i}(w_i) \mathbf{z}_{|i} \mid W_i = w_i \} = H_{|i}(\mathbf{z}_{|i}), \quad (5.1)$$

for non-degenerate distribution functions $H_{|i}$, $i \in \{1, \dots, d\}$, where \mathbf{W}_{-i} denotes the vector \mathbf{W} with the i^{th} component removed. Here, $\mathbf{z}_{|i}$ is within the support of the residual random vector

$$\mathbf{Z}_{|i} = (\mathbf{W}_{-i} - \mathbf{a}_{|i}(w_i)) / \mathbf{b}_{|i}(w_i) \sim H_{|i}. \quad (5.2)$$

A direct consequence of assumption (5.1) is that, conditional on $W_i > u_i$, the variables $W_i - u_i$

and $\mathbf{Z}_{|i}$ are independent in the limit as $u_i \rightarrow \infty$, with limiting distributions as unit exponential and $H_{|i}$, respectively.

Parametric families for the normalising functions $\mathbf{a}_{|i}$ and $\mathbf{b}_{|i}$ were provided for the case of Laplace margins by Keef et al. (2013). Specifically, they set

$$\mathbf{a}_{|i}(w_i) = \boldsymbol{\alpha}_{-|i} w_i \quad \text{and} \quad \mathbf{b}_{|i}(w_i) = w_i^{\boldsymbol{\beta}_{-|i}}, \quad (5.3)$$

for $\boldsymbol{\alpha}_{-|i} \in [-1, 1]^{d-1}$ and $\boldsymbol{\beta}_{-|i} \in (-\infty, 1]^{d-1}$, with vector operations applied componentwise. Let $\alpha_{j|i}$ and $\beta_{j|i}$, $j \in \{1, \dots, d\} \setminus \{i\}$, denote the elements of the respective parameter vectors associated with variable W_j .

Estimation of the $\boldsymbol{\alpha}_{-|i}$ and $\boldsymbol{\beta}_{-|i}$ can be achieved via standard maximum likelihood techniques, provided we make an additional assumption regarding the parametric form of the distribution $H_{|i}$. Accepted practice is to assume IID marginal distributions $H_{j|i} \sim N(\mu_j, \sigma_j^2)$, $\mu_j \in \mathbb{R}$, $\sigma_j \in \mathbb{R}_+$ for all $j \in \{1, \dots, d\} \setminus \{i\}$, as suggested by Heffernan and Tawn (2004).

Having obtained maximum likelihood estimates for $\boldsymbol{\alpha}_{-|i}$, $\boldsymbol{\beta}_{-|i}$ for some high threshold u_i of W_i , extreme predictions in the form of $(\mathbf{W}_{-i}, W_i) | W_i > v_i$ can be made for any $v_i \geq u_i$, by exploiting the limiting independence of $(W_i - v_i)$ and $\mathbf{Z}_{|i}$. Drawing a realisation $\mathbf{z}_{|i}$ of $\mathbf{Z}_{|i}$ from the set of fitted residual values (5.2) and independently generating an observation from $(W_i - v_i)$ provides a new observation of \mathbf{W} in the region $\{\mathbf{w} \in \mathbb{R}^d; w_i > v_i\}$. Algorithm 1 details how we employ this method when estimating extreme set probabilities.

We apply the above methodology when estimating probabilities p_1 and p_2 defined in Section 5.1. The analysis of Section 5.1 identified five subgroups G_1, \dots, G_5 , between which we assume independence. As is discussed in Section 5.1, we leverage this dependence pattern when estimating probabilities p_1 and p_2 by calculating the individual subgroup probabilities separately.

We first transform the data onto Laplace margins via $W_i := F_L(F_G^{-1}(Y_i))$, where F_G and F_L denote standard Gumbel and Laplace distribution functions, respectively. Setting $\mathbf{W} := (W_1, \dots, W_{50})$, we divide this random vector into the five subgroups identified in Section 5.1. The subgroup probabilities are each estimated using Algorithm 1 for each subvector. For this,

Algorithm 1 Extremal probability estimation using conditional extremes

- 1: Fit the conditional extremes model as described above.
- 2: Select a number $N \in \mathbb{Z}^+$ of values to generate.
- 3: **for** $j \in \{1 \dots, N\}$ **do**
- 4: Simulate a realisation w_i of $(W_i - v_i) | (W_i > v_i)$ from a unit exponential distribution.
- 5: Sample $\mathbf{z}_{|i}$ from the set of fitted residual values (5.2).
- 6: Set $\mathbf{w}_{-i} = \boldsymbol{\alpha}_{-i} w_i + \boldsymbol{\beta}_{-i}^{w_i} \mathbf{z}_{|i}$.
- 7: Obtain a realisation $\mathbf{w}^j := (\mathbf{w}_{-i}, w_i)$ of $(\mathbf{W}_{-i}, W_i) | W_i > v_i$.
- 8: **end for**
- From this we obtain realisations $\{\mathbf{w}^j\}_{j=1}^N$.*
- 9: Estimate the probability $\Pr(\mathbf{W} \in A)$ for $A \subset \{\mathbf{x} \in \mathbb{R}^d; x_i > v_i\}$ via

$$\hat{p}_A = \left(\frac{1}{N} \sum_{j=1}^N \mathbb{1}(\mathbf{w}^j \in A) \right) \left(\frac{1}{2} \exp(-v_i) \right),$$

where the right-side term originates from the unit Laplace marginal exceedance probability.

we select the first element of each subvector as the conditioning variable and simulate 10^8 replicates from each fitted model to obtain probability estimates. To account for uncertainty in the estimation of the normalising functions (5.3), we perform a parametric bootstrapping procedure with 100 samples. That is, we fit an initial conditional extremes model for a given conditioning threshold, then use this model to generate 100 predictive samples and apply Algorithm 1 to each to estimate 100 realisations of the target probabilities. Sensitivity analyses of the estimated probabilities to the choice of conditioning variable suggest no significant effect. Furthermore, we consider a range of conditioning thresholds; the corresponding estimates of subgroup probabilities defined in Section 5.1 appear relatively stable with respect to the conditioning threshold quantile. We ultimately select 0.85-quantiles for the conditioning thresholds of our final probability estimates.

5.3 Results

Figure 6 shows the bootstrapped estimated individual group and overall probabilities with respect to conditioning threshold quantile for part 1. The results for part 2 are given in the Supplementary

Material. Our final estimates are given by $\hat{p}_1 = 1.093634 \times 10^{-26} (2.149591 \times 10^{-36}, 1.359469 \times 10^{-24})$ and $\hat{p}_2 = 1.075787 \times 10^{-31} (1.596381 \times 10^{-46}, 1.850425 \times 10^{-29})$, with 95% confidence intervals given in parentheses.

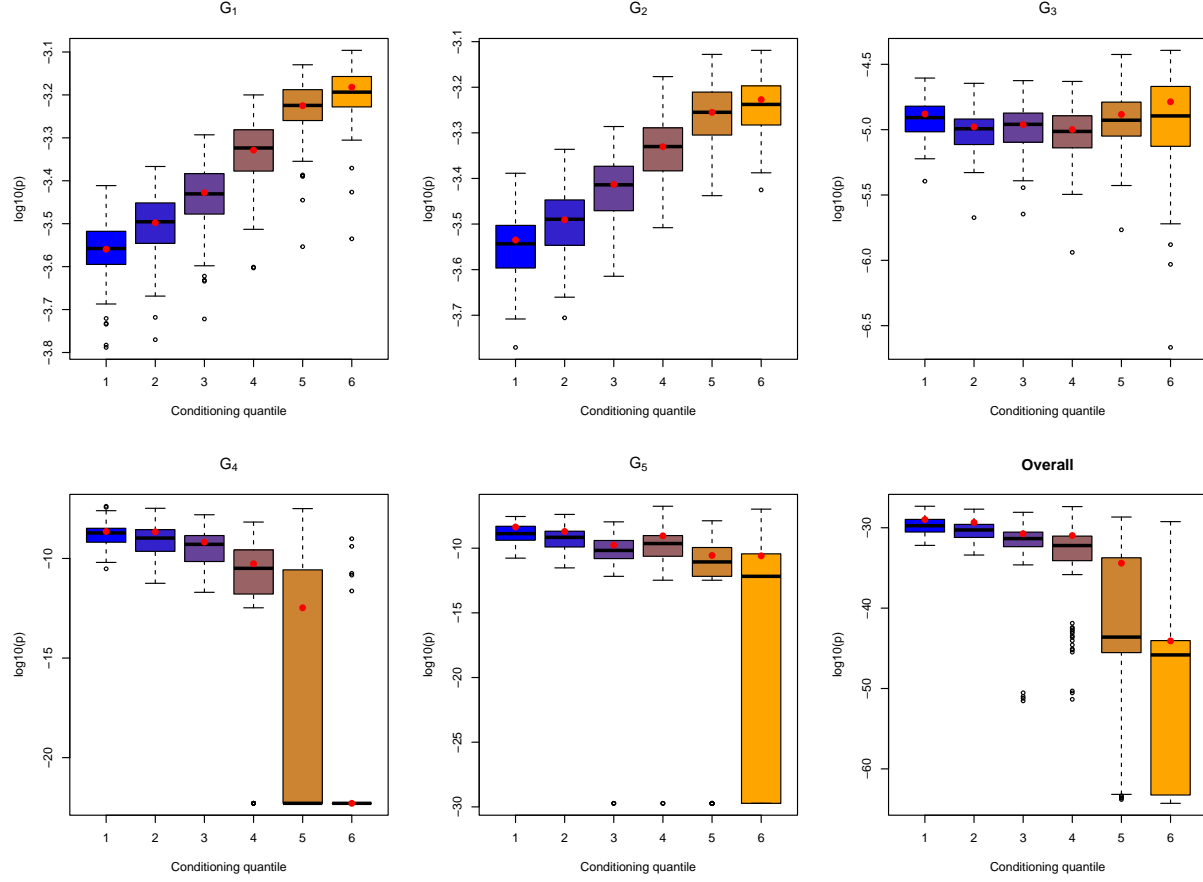


Figure 6: Part 1 subgroup and overall bootstrapped probability estimates on the log scale. The red points indicate the original sample estimates and the colouring of the boxplots indicates the choice of conditioning threshold, with the conditioning quantile indices 1-6 referring to the quantile levels $\{0.7, 0.75, 0.8, 0.85, 0.9, 0.95\}$, respectively.

6 Discussion

In this paper, we have proposed a range of statistical methods for estimating extreme quantities for challenges C1-C4. For the univariate challenge C1, we estimate an extremal quantile for a response conditioned on a set of environmental covariates. Specifically we wanted to estimate the 0.9999-quantile, and the associated 50% confidence intervals, of $Y \mid \mathbf{X} = \mathbf{x}_i, i \in \{1, \dots, n\}$. For

challenge C2, we estimated a quantile, corresponding to a once in 200 year level, of the marginal distribution Y whilst incorporating the loss function in equation (3.2). Overall we ranked 6th and 4th for challenges C1 and C2, respectively.

For challenge C1, our final model (model 7 in Table 1) was chosen to minimise the model selection criteria but the QQ plot under-estimates the most extreme values of the response (see Figure 2). Despite this under-estimation, the conditional quantiles calculated for C1 are generally well aligned with the true quantiles. If we ignore the model selection criteria and chose the model based on a visual assessment of QQ plots, we would have chosen model 5 in Table 1 and this would have covered the true quantile on fewer occasions than our chosen model. Therefore, the main issue with our results is the narrow confidence intervals.

Narrow confidence intervals are an indication of over-fitting and this could have arisen in several places. For instance, Rohrbeck et al. (2023) suggested all the seasonality is captured in the threshold, while our model includes a seasonal threshold and a covariate for seasonality in the scale parameter of the GPD model. As well as over-fitting, the model may not have been flexible enough. This could be, in part, due to our model missing covariates. For instance, the true model contained V_2 as a covariate (Rohrbeck et al., 2023) whilst our model did not. In addition, the basis dimensions for our splines are low. In practice, one should choose a higher dimension than we would expect and although we chose the dimension using a model-based approach, it may have resulted in the splines not being flexible enough to capture all of the trends in the data. Since we used the same model for challenges C1 and C2, these issues can also be attributed to our ranking in C2.

For the first multivariate challenge C3, we employ an extension of Wadsworth and Tawn (2013) to estimate the probability of three variables lying in an extremal set. Our extension to this framework accounts for non-stationarity in the data when estimating the associated coefficient which relies on GAMs to obtain the parameters. The QQ plots for the resulting fitted exceedance model suggested a reasonable fit; however, parameter estimates show the proposed modelling

approach was not the most suitable. For this challenge, we ranked 5th and our estimates are on the same order of magnitude as the truth (Rohrbeck et al., 2023).

We note similarities in the methodologies presented for the challenges C1, C2, and C3. Specifically, each of the proposed methods used the EVGAM framework for capturing non-stationary tail behaviour via a generalised Pareto distribution. We acknowledge that the model selection tool proposed for C1 and C2 could also be applied for C3. However, we opted not to use this tool for several reasons. Firstly, unlike the univariate setting, there is no guarantee of convergence to a GPD in the limit, and the GPD tail assumption thereby needs to be tested. Moreover, in exploratory analysis, we tested the model selection tool for C3 but found the selected models and quantiles to not be satisfactory, particularly in the upper tail of the min-projection. We therefore select a model manually, using QQ plots to evaluate performance. Exploring threshold and model selection techniques for multivariate extremes represents an important area of research.

In the final multivariate challenge C4, we were asked to estimate very high-dimensional joint survival probabilities. To do so, we split the probability into 5 lower-dimensional asymptotically independent components, then estimated each using the conditional extremes method of Heffernan and Tawn (2004). In the final rankings of Rohrbeck et al. (2023), we ranked 3rd for this challenge. A more prudent method could have been implemented, as groups of variables were never truly independent. Alternatively, we could consider estimating individual group probabilities across varying thresholds and then taking an average value as our final result. Even though sensitivity analyses indicate little effect of thresholds on model parameter estimates, it may have had a more significant impact on final probability estimates.

Declarations

Funding

This work was supported by EPSRC grant numbers EP/L015692/1, EP/S022252/1, EP/W523811/1 and EP/W524438/1, and SFI grant number 18/CRT/6049.

Competing interests

The authors have no relevant financial or non-financial interests to disclose.

Data availability

The data that support the findings of this study are available from the corresponding author upon reasonable request.

Ethical Approval

Not Applicable

Authors' contributions

All authors contributed equally to this work.

Acknowledgments

This paper is based on work completed while Lúdia André, Eleanor D'Arcy, Conor Murphy, Callum Murphy-Barltrop and Matthew Speers were part of the EPSRC funded STOR-i centre for doctoral training (EP/L015692/1, EP/S022252/1), Ryan Campbell, Aiden Farrell and Lydia Kakampakou were part of EPSRC funded projects (EP/W523811/1, EP/W524438/1), and Dáire Healy was part of the Science Foundation Ireland funded project (18/CRT/6049). We would like

to especially thank Ben Youngman for his assistance with the `evgam` package in the R computing language, alongside Christian Rohrbeck, Emma Simpson and Jonathan Tawn for their hard work in organising the data challenge.

References

- Chavez-Demoulin, V. and Davison, A. C. (2005). Generalized additive modelling of sample extremes. *Journal of the Royal Statistical Society: Series C (Applied Statistics)*, 54:207–222.
- Davison, A. C. and Smith, R. L. (1990). Models for Exceedances Over High Thresholds. *Journal of the Royal Statistical Society. Series B: Statistical Methodology*, 52:393–425.
- D’Arcy, E., Tawn, J. A., Joly, A., and Sifnioti, D. E. (2023). Accounting for seasonality in extreme sea-level estimation. *The Annals of Applied Statistics*, 17(4):3500–3525.
- Eastoe, E. F. and Tawn, J. A. (2009). Modelling non-stationary extremes with application to surface level ozone. *Journal of the Royal Statistical Society. Series C: Applied Statistics*, 58:25–45.
- Engelke, S. and Ivanovs, J. (2021). Sparse Structures for Multivariate Extremes. *Annual Review of Statistics and Its Application*, 8:241–270.
- Gneiting, T. and Katzfuss, M. (2014). Probabilistic forecasting. *Annual Review of Statistics and Its Application*, 1:125–151.
- Guerrero, M. B., Huser, R., and Ombao, H. (2023). Conex–Connect: Learning patterns in extremal brain connectivity from MultiChannel EEG data. *The Annals of Applied Statistics*, 17:178–198.
- Harrison, E., Drake, T., and Ots, R. (2023). *finalfit: Quickly Create Elegant Regression Results Tables and Plots when Modelling*. R package version 1.0.7.

- Hastie, T., Tibshirani, R., and Friedman, J. (2001). *The Elements of Statistical Learning*. Springer, New York.
- Heffernan, J. E. and Tawn, J. A. (2004). A conditional approach for multivariate extreme values. *Journal of the Royal Statistical Society. Series B: Statistical Methodology*, 66:497–546.
- Hill, B. M. (1975). A Simple General Approach to Inference About the Tail of a Distribution. *The Annals of Statistics*, 3:1163–1174.
- Joe, H. (1997). *Multivariate Models and Multivariate Dependence Concepts*. Chapman and Hall/CRC.
- Jonathan, P., Randell, D., Wu, Y., and Ewans, K. (2014). Return level estimation from non-stationary spatial data exhibiting multidimensional covariate effects. *Ocean Engineering*, 88:520–532.
- Keef, C., Papastathopoulos, I., and Tawn, J. A. (2013). Estimation of the conditional distribution of a multivariate variable given that one of its components is large: Additional constraints for the Heffernan and Tawn model. *Journal of Multivariate Analysis*, 115:396–404.
- Killick, R. and Eckley, I. (2014). changepoint: An R package for changepoint analysis. *Journal of statistical software*, 58(3):1–19.
- Kyselý, J., Pícek, J., and Beranová, R. (2010). Estimating extremes in climate change simulations using the peaks-over-threshold method with a non-stationary threshold. *Global and Planetary Change*, 72:55–68.
- Ledford, A. W. and Tawn, J. A. (1996). Statistics for near independence in multivariate extreme values. *Biometrika*, 83:169–187.
- Mhalla, L., Opitz, T., and Chavez-Demoulin, V. (2019). Exceedance-based nonlinear regression of tail dependence. *Extremes*, 22:523–552.

- Murphy, C., Tawn, J. A., and Varty, Z. (2023). Automated threshold selection and associated inference uncertainty for univariate extremes. *arXiv*, 2310.17999.
- Murphy-Barltrop, C. J. R. and Wadsworth, J. L. (2022). Modelling non-stationarity in asymptotically independent extremes. *arXiv*, 2203.05860.
- Murphy-Barltrop, C. J. R., Wadsworth, J. L., and Eastoe, E. F. (2023). Improving estimation for asymptotically independent bivariate extremes via global estimators for the angular dependence function. *arXiv*, 2303.13237.
- Northrop, P. J., Attalides, N., and Jonathan, P. (2017). Cross-validatory extreme value threshold selection and uncertainty with application to ocean storm severity. *Journal of the Royal Statistical Society. Series C: Applied Statistics*, 66:93–120.
- Northrop, P. J. and Jonathan, P. (2011). Threshold modelling of spatially dependent non-stationary extremes with application to hurricane-induced wave heights. *Environmetrics*, 22:799–809.
- Pickands, J. (1975). Statistical Inference Using Extreme Order Statistics. *The Annals of Statistics*, 3:119–131.
- Politis, D. N. and Romano, J. P. (1994). The Stationary Bootstrap. *Journal of the American Statistical Association*, 89:1303–1313.
- Quinn, N., Bates, P. D., Neal, J., Smith, A., Wing, O., Sampson, C., Smith, J., and Heffernan, J. (2019). The Spatial Dependence of Flood Hazard and Risk in the United States. *Water Resources Research*, 55:1890–1911.
- Resnick, S. (2002). Hidden Regular Variation, Second Order Regular Variation and Asymptotic Independence. *Extremes*, 5:303–336.

- Rohrbeck, C., Simpson, E. S., and Tawn, J. A. (2023). Editorial: EVA 2023 Data Challenge. *Extremes*, (to appear).
- Scarrott, C. and MacDonald, A. (2012). A review of extreme value threshold estimation and uncertainty quantification. *Revstat Statistical Journal*, 10:33–60.
- Schneider, L. F., Krajina, A., and Krivobokova, T. (2021). Threshold selection in univariate extreme value analysis. *Extremes*, 24:881–913.
- Simpson, E. S., Wadsworth, J. L., and Tawn, J. A. (2020). Determining the dependence structure of multivariate extremes. *Biometrika*, 107:513–532.
- Tawn, J. A. (1988). Bivariate extreme value theory: Models and estimation. *Biometrika*, 75:397–415.
- Wadsworth, J. L. and Tawn, J. A. (2013). A new representation for multivariate tail probabilities. *Bernoulli*, 19:2689–2714.
- Wadsworth, J. L., Tawn, J. A., Davison, A. C., and Elton, D. M. (2017). Modelling across extremal dependence classes. *Journal of the Royal Statistical Society. Series B: Statistical Methodology*, 79:149–175.
- Wood, S. N. (2017). *Generalized Additive Models*. Chapman and Hall/CRC.
- Youngman, B. D. (2019). Generalized Additive Models for Exceedances of High Thresholds With an Application to Return Level Estimation for U.S. Wind Gusts. *Journal of the American Statistical Association*, 114:1865–1879.
- Youngman, B. D. (2022). evgam: An R Package for Generalized Additive Extreme Value Models. *Journal of Statistical Software*, 103(3):1–26.
- Yu, K. and Moyeed, R. A. (2001). Bayesian quantile regression. *Statistics & Probability Letters*, 54:437–447.

Supplementary Material to “Extreme value methods for estimating rare events in Utopia”

S1 Additional figures for Section 2

In this section, we present additional figures for Section 2 of the main paper, concerned challenges C1 and C2. Figures S1-S4 support the exploratory analysis for challenges C1 and C2. We explore the within-year seasonality of the response variable Y in Figure S1, looking at the distribution of Y per month and across the two seasons. This shows that there is a significant difference in the distribution of Y between seasons 1 and 2, but within each season there is little difference across months.

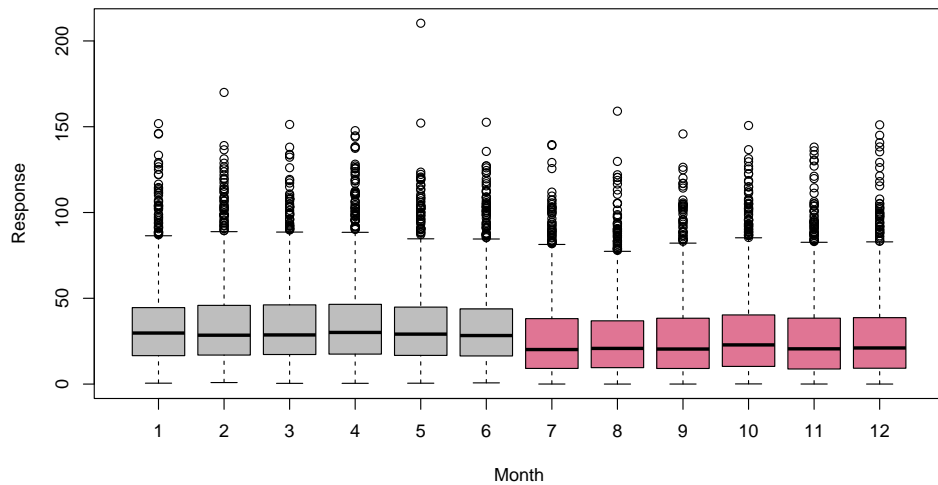


Figure S1: Box plot of the response variable Y with each month and season (season 1 in grey and season 2 in red).

Figure S2 shows a scatter plot of Y against each covariate V_1, \dots, V_8 , excluding V_6 with corresponds to season. Covariates V_1, V_2 and V_8 do not seem to have a relationship with Y , whilst there appears to be dependence for the remaining covariates. These observed relationships appear complex and non-linear.

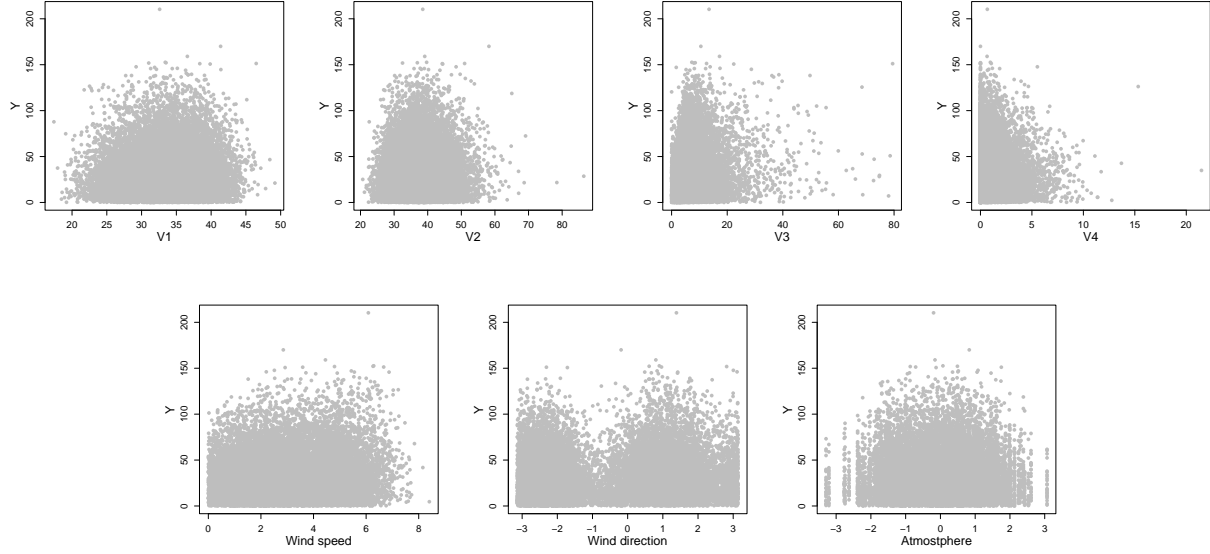


Figure S2: Scatter plots of explanatory variables V_1, \dots, V_4 , wind speed (V_6), wind direction (V_7) and atmosphere (V_8), from top-left to bottom-right (by row), against the response variable Y .

Figure S3 shows wind rose plots before and after the changepoint we find for V_6 (wind speed) and V_7 (wind direction). These graphs demonstrate the direction of wind observed, as well as the speeds for each direction (divided into eight sectors). We find that wind speeds are greater before the changepoint, and mostly come from the south-westerly direction. Whilst after the changepoint, winds tend to come from the north-easterly direction and with lower speeds.

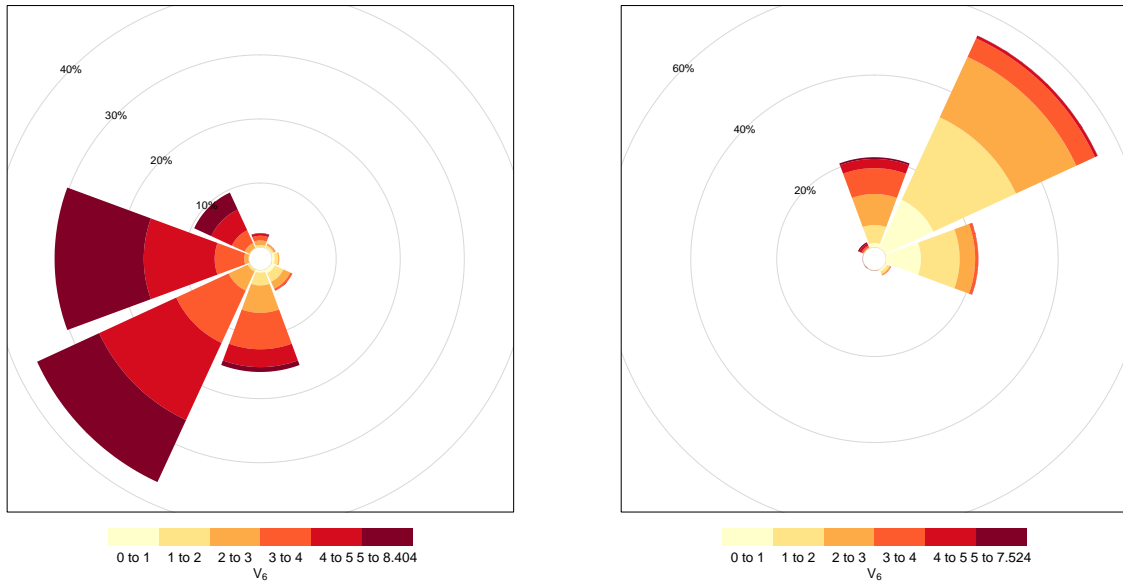


Figure S3: Wind rose plot before (left) and after (right) the changepoint.

Figure S4 details the auto-correlation function (acf) values for the response Y and explanatory variables $V_1, \dots, V_4, V_6, \dots, V_8$, up to a lag of 60. All variables have negligible acf values beyond lag 0, except V_6 (wind speed), V_7 (wind direction) and V_8 (atmosphere).

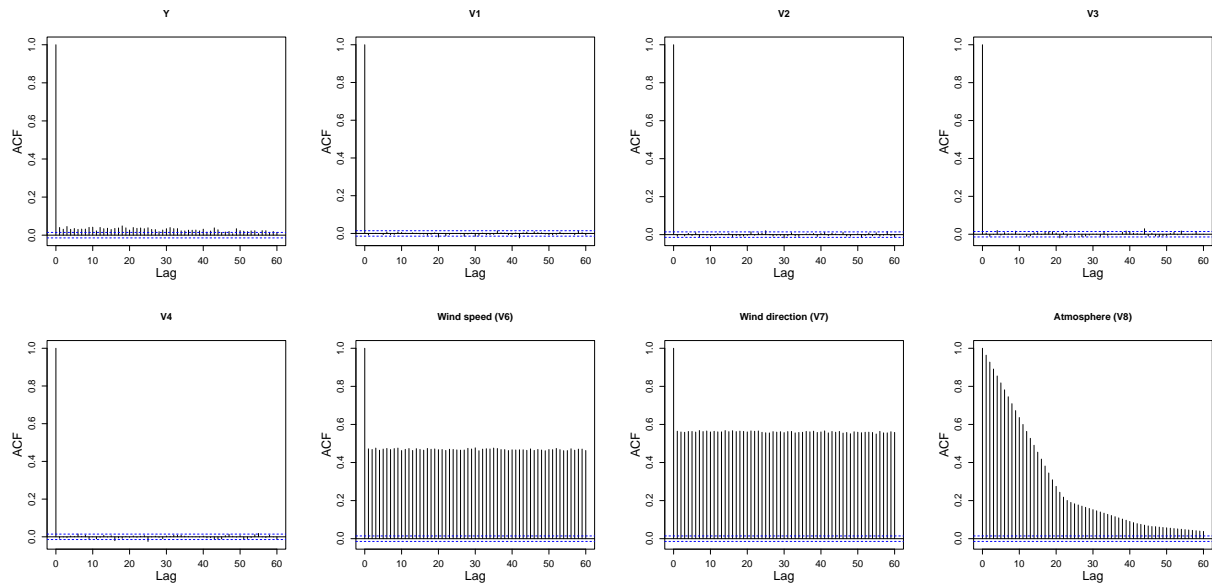


Figure S4: Autocorrelation function plots for the response variable Y and explanatory variables V_1, \dots, V_4 , wind speed (V_6), wind direction (V_7) and atmosphere (V_8), from top-left to bottom-right (by row), against the response variable Y .

Figure S5 shows the QQ-plots corresponding to a standard GPD model fitted to the excesses of Y above a constant (left) and seasonally-varying threshold (right). 95% tolerance bounds (grey) show a lack of agreement between observations and the standard GPD model above a constant threshold. The second plot demonstrates a significant improvement in model fit.

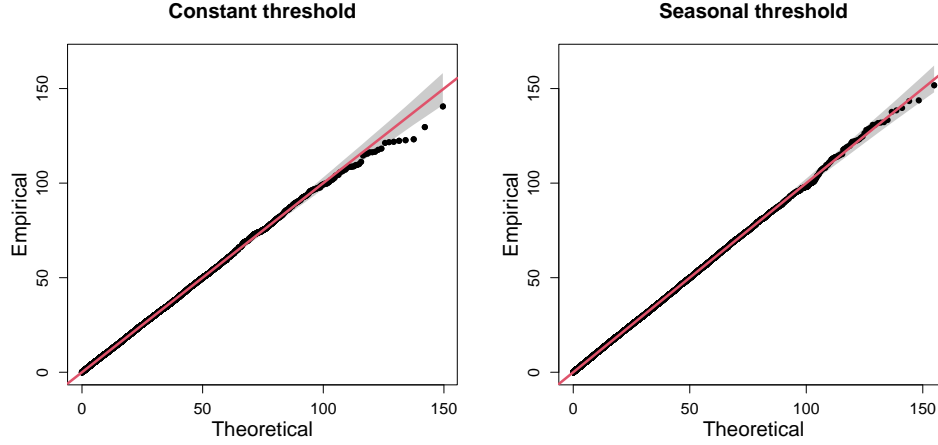


Figure S5: QQ-plots showing standard GPD model fits with 95% tolerance bounds (grey) above a constant (left) and stepped-seasonal (right) threshold.

Figure S6 shows a detailed summary of the pattern of missing data in the data and can be produced using the `missing_pattern` function in the `finalfit` package in R (Harrison et al., 2023). To interpret the figure note that blue and red squares represent observed and missing variables, respectively. The number on the right indicates the number of missing random variables (i.e., the number of red squares in the row), while the number on the left is the number of observations that fall into the row category. On the bottom, we have the number of observations that fall into the column category. For example, 18,545 observations are fully observed (denoted by the first row), there are 407 observations where only V_4 is missing (denoted by the second row), there are 13 observations where both V_4 and V_6 are missing (denoted by the fourth row), there are 456 observations where V_4 and at least one other predictor is missing (denoted by the last column in the table) etc. It can be seen that there are very few observations where more than one predictor is missing.

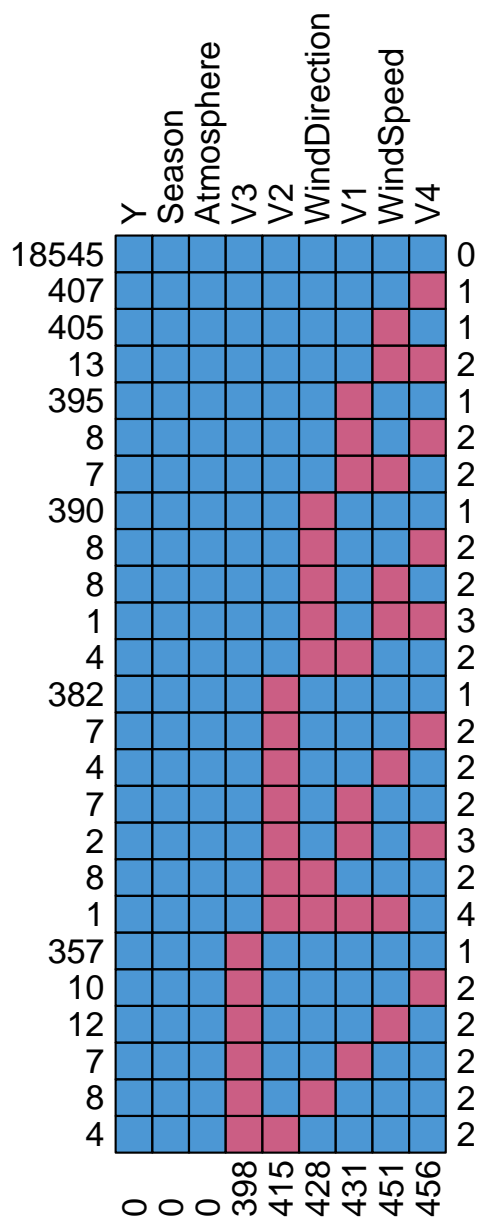


Figure S6: Detailed pattern of missing predictor variables in the Amaurot data set.

S2 Additional figures for Section 3

In this section, we present additional plots related to Section 3 of the main article. Figure S7 illustrates the time series of both covariates for the first 3 years of the observation period. One can observe how the seasons vary periodically over each year, as well as the discrete nature of the atmospheric covariate.

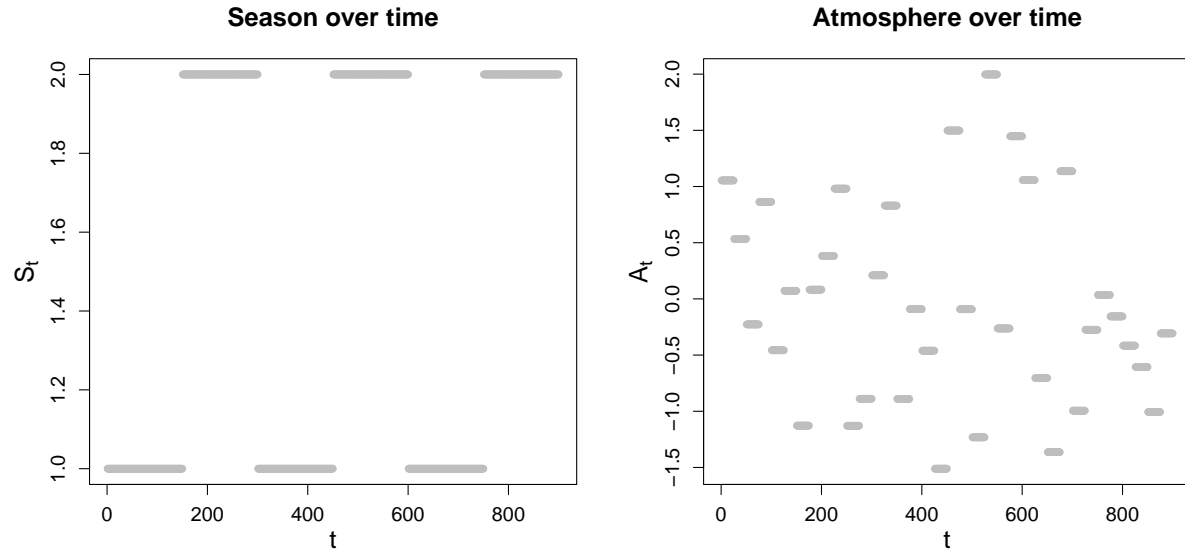


Figure S7: Plots of S_t (left) and A_t (right) against t for the first 3 years of the observation period.

Bootstrapped χ estimates for the groups $G_{I,k}^A, k \in \{1, \dots, 10\}, I \in \mathcal{I} \setminus \{1, 2, 3\}$ and $G_{I,k}^S, k \in \{1, 2\}, I \in \mathcal{I}$ are given in Figures S8 - S11. These estimates illustrate the impact of atmosphere on the dependence structure.

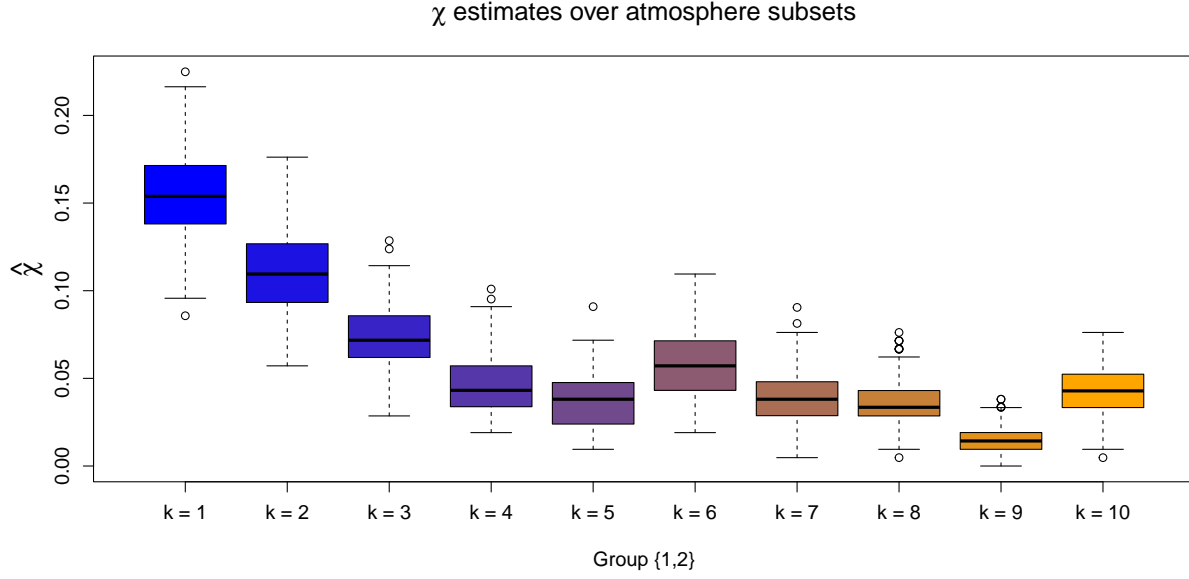


Figure S8: Boxplots of empirical χ estimates obtained for the subsets $G_{I,k}^A$, with $k = 1, \dots, 10$ and $I = \{1, 2\}$. The colour transition (from blue to orange) over k illustrates the trend in χ estimates as the atmospheric values are increased.

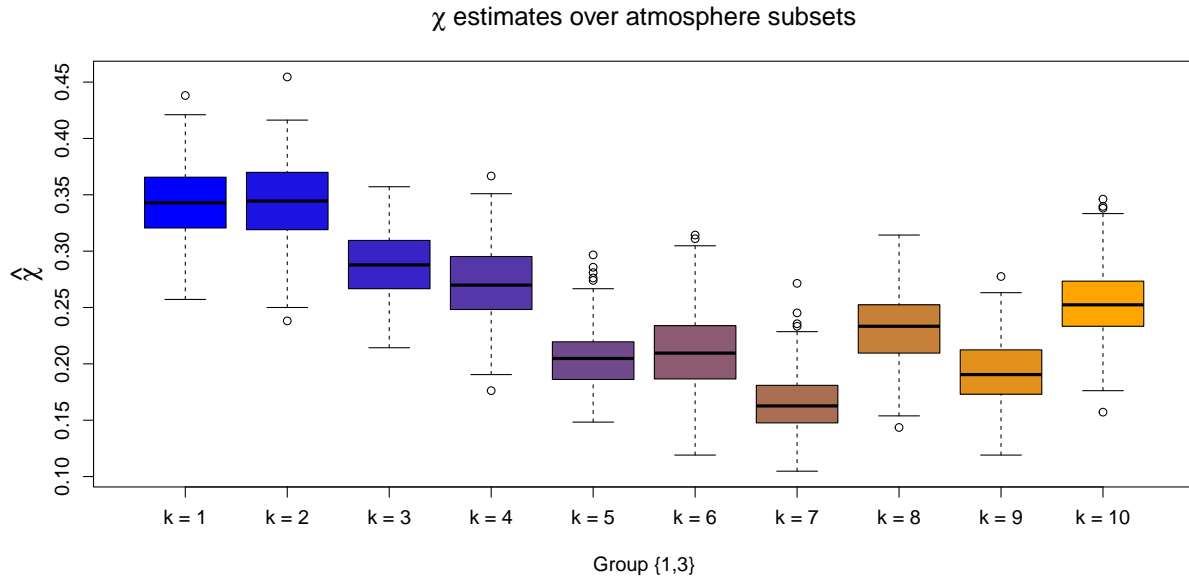


Figure S9: Boxplots of empirical χ estimates obtained for the subsets $G_{I,k}^A$, with $k = 1, \dots, 10$ and $I = \{1, 3\}$. The colour transition (from blue to orange) over k illustrates the trend in χ estimates as the atmospheric values are increased.

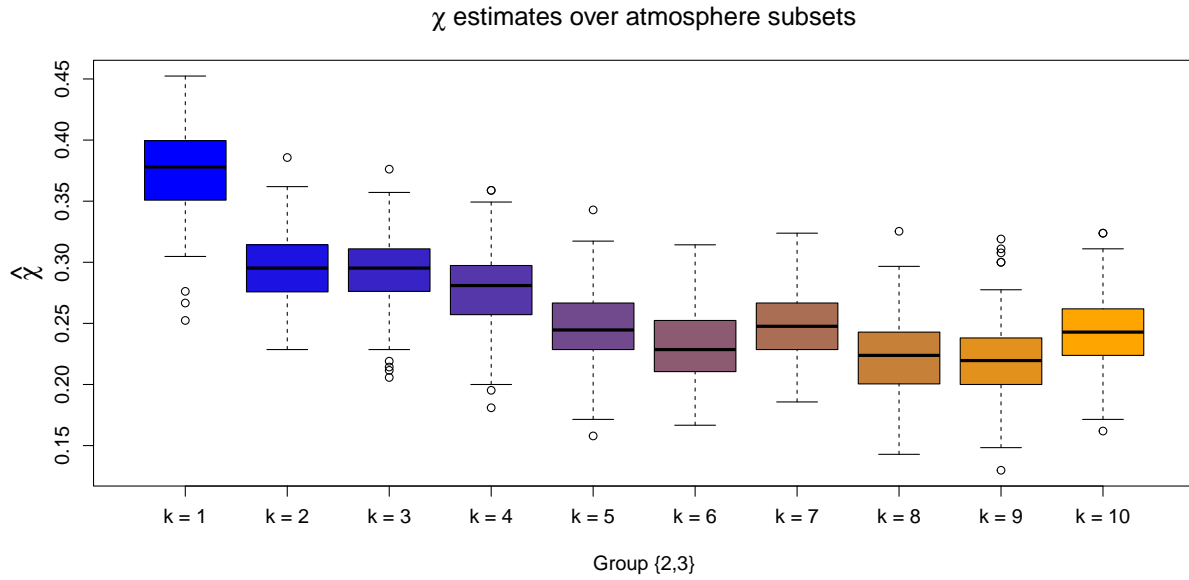


Figure S10: Boxplots of empirical χ estimates obtained for the subsets $G_{I,k}^A$, with $k = 1, \dots, 10$ and $I = \{2, 3\}$. The colour transition (from blue to orange) over k illustrates the trend in χ estimates as the atmospheric values are increased.

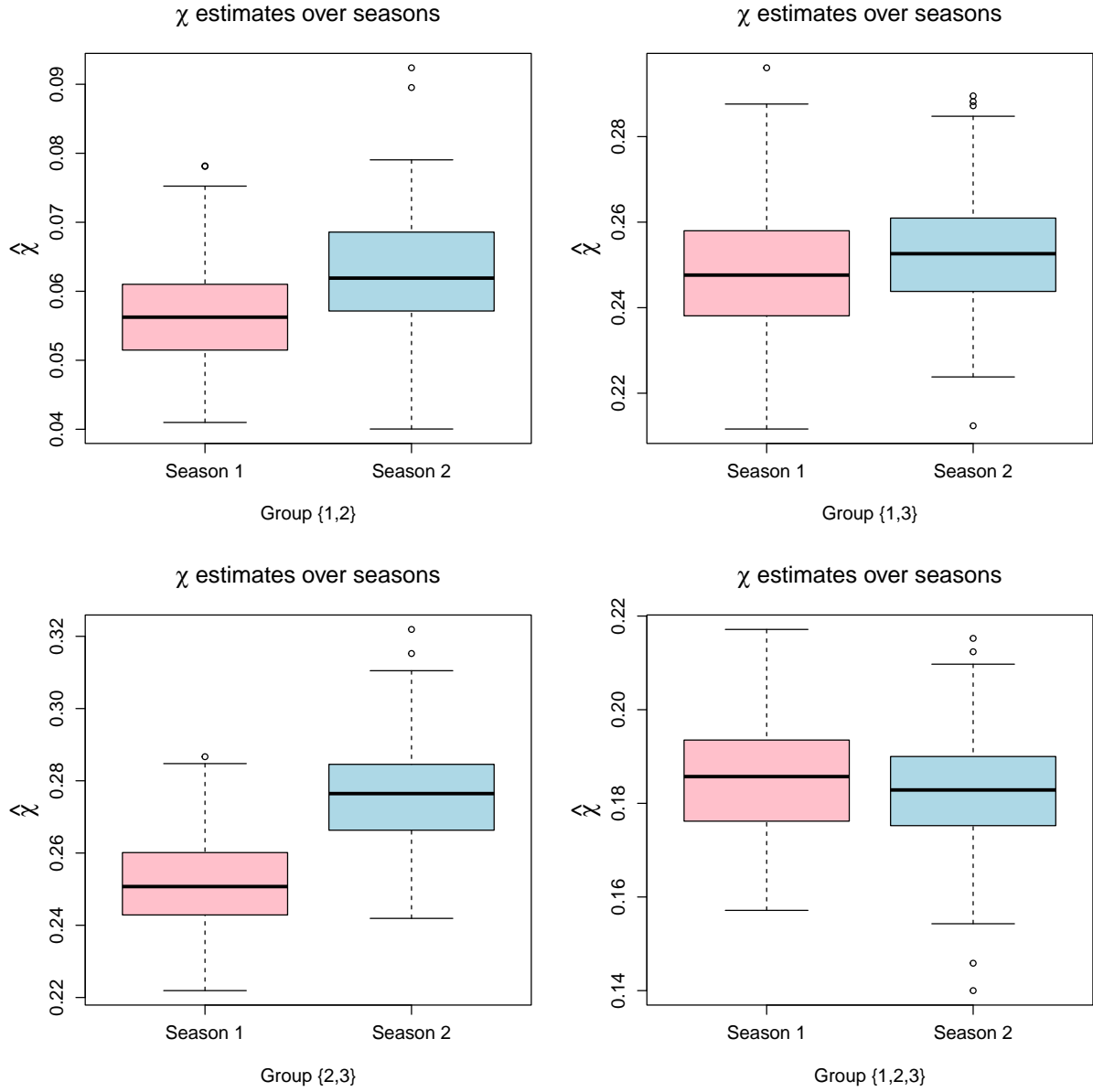


Figure S11: Boxplots of empirical χ estimates obtained for the subsets $G_{I,k}^S$, with $k = 1, 2$. In each case, pink and blue colours illustrate estimates for seasons 1 and 2, respectively. From top left to bottom right: $I = \{1, 2, 3\}$, $I = \{1, 2\}$, $I = \{1, 3\}$, $I = \{2, 3\}$.

For a 3-dimensional random vector, the angular dependence function, denoted λ , is defined on the unit-simplex S^2 and describes extremal dependence along different rays $\omega \in S^2$. As noted in Section 4.2 of the main manuscript, we can associate each of the probabilities from C3, p_1 and p_2 , with points on S^2 , denoted ω^1 and ω^2 respectively. With $I = \{1, 2, 3\}$, we consider $\lambda(\omega^1)$ and $\lambda(\omega^2)$ over the subsets $G_{I,k}^S$, $k \in \{1, 2\}$ and $G_{I,k}^A$, $k \in \{1, \dots, 10\}$. We note that $\lambda(\omega^1)$ is analogous with the coefficient of tail dependence $\eta \in (0, 1]$ (Ledford and Tawn, 1996), with $\eta = 1/3\lambda(\omega^1)$; this corresponds with the region where all variables are simultaneously extreme. Furthermore, $\lambda(\omega^2)$, which corresponds to a region where only two variables are extreme, is only evaluated after an additional marginal transformation of the third Coputopia time series; see Section 4.2 of the main manuscript.

Estimation of λ for each simplex point and subset was achieved using the Hill estimator (Hill, 1975) at the 90% level, with uncertainty subsequently quantified via bootstrapping. These results are given in Figures S12 - S15. These plots provide further evidence of a relationship between the extremal dependence structure and the covariates.

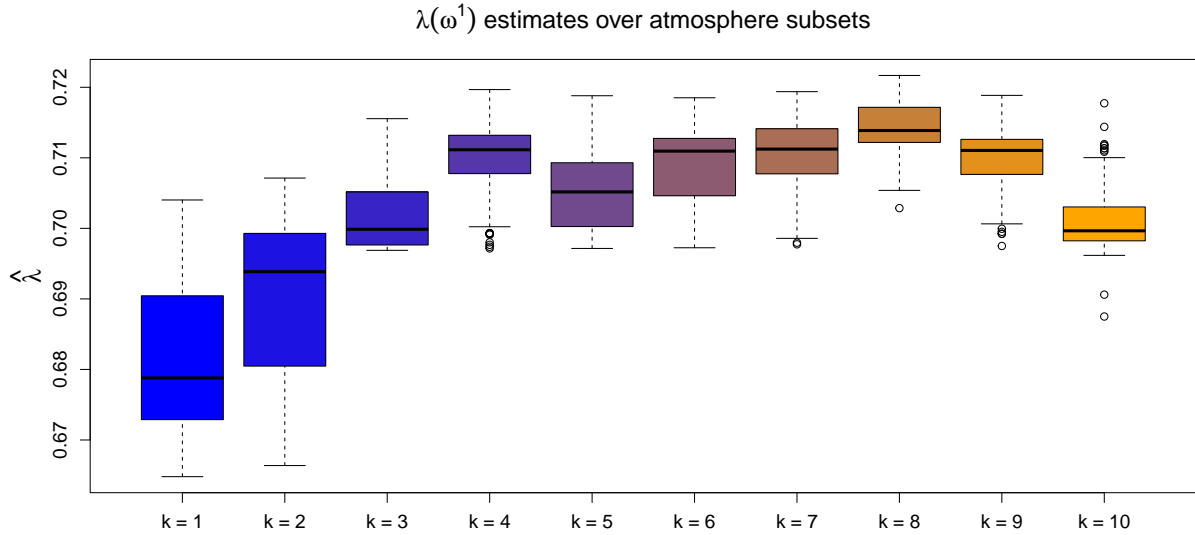


Figure S12: Boxplots of empirical $\lambda(\omega_i)$ estimates obtained for the subsets $G_{I,k}^A$, with $k = 1, \dots, 10$ and $I = \{1, 2, 3\}$. The colour transition (from blue to orange) over k illustrates the trend in λ estimates as the atmospheric values are increased.

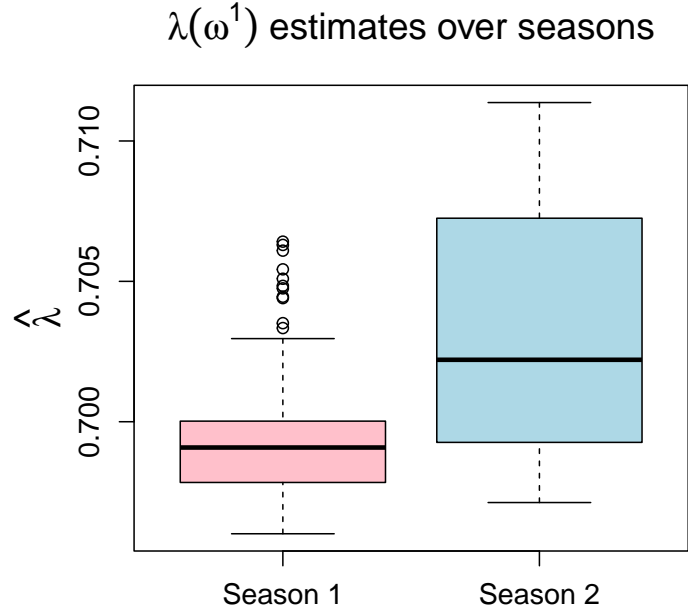


Figure S13: Boxplots of empirical $\lambda(\omega_i)$ estimates obtained for the subsets $G_{I,k}^S$, with $k = 1, 2$ and $I = \{1, 2, 3\}$. In each case, pink and blue colours illustrate estimates for seasons 1 and 2, respectively.

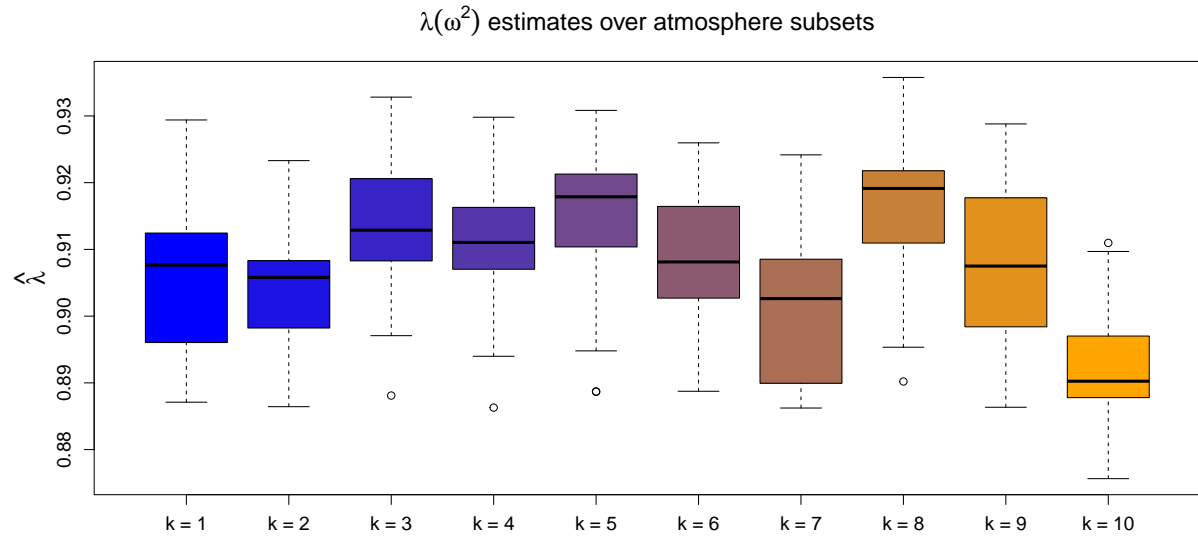


Figure S14: Boxplots of empirical $\lambda(\omega_{ii})$ estimates obtained for the subsets $G_{I,k}^A$, with $k = 1, \dots, 10$ and $I = \{1, 2, 3\}$. The colour transition (from blue to orange) over k illustrates the trend in λ estimates as the atmospheric values are increased.

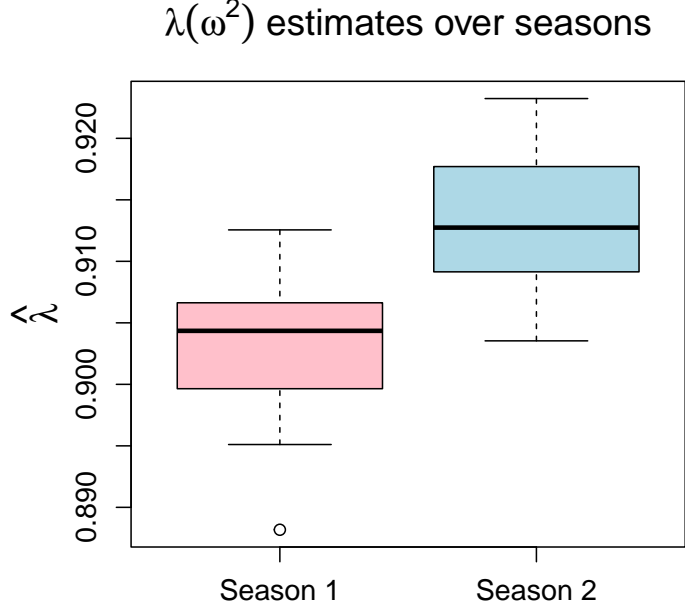


Figure S15: Boxplots of empirical $\lambda(\omega_{ii})$ estimates obtained for the subsets $G_{I,k}^S$, with $k = 1, 2$ and $I = \{1, 2, 3\}$. In each case, pink and blue colours illustrate estimates for seasons 1 and 2, respectively.

To illustrate the estimated trend in dependence, Figure S16 illustrates the estimated scale functions, $\sigma(\omega \mid \mathbf{x}_t)$, over atmosphere for parts 1 and 2. Under the assumption of asymptotic normality in the spline coefficients, 95% confidence intervals are obtained via posterior sampling; see Wood (2017) for more details. We observe that σ tends to increase and decrease over atmosphere for parts 1 and 2, respectively, although the trend is less pronounced for the latter. Under our modelling framework, we note that higher values of σ are associated with less positive extremal dependence in the direction ω of interest; to see this, observe that the survivor function of the GPD with fixed ξ is negatively associated with σ . Considering the trend in $\sigma(\omega \mid \mathbf{x}_t)$, our results indicate a decrease in dependence in the region where all variables are extreme.

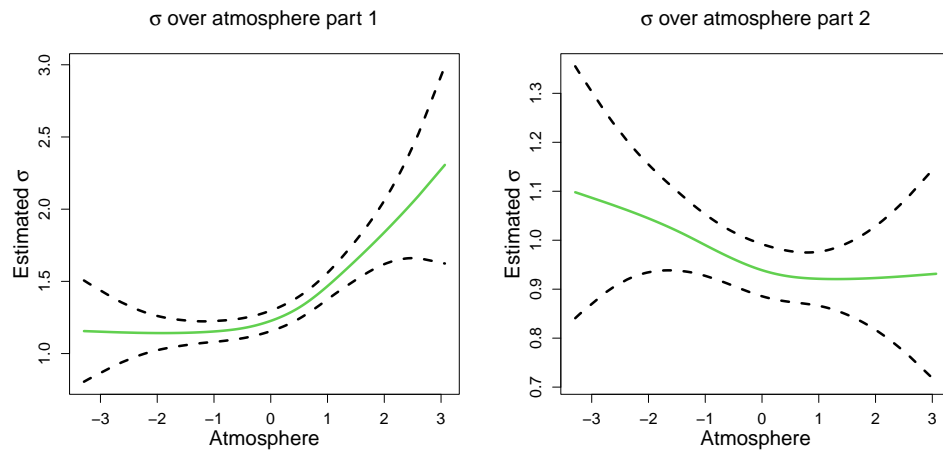


Figure S16: Estimated σ functions (green) over atmosphere for part 1 (left) and 2 (right). In both cases, the regions defined by the black dotted lines represent 95% confidence intervals obtained using posterior sampling.

S3 Additional figures for Section 4

Figure S17 shows a heat map of empirically estimated $\eta(\cdot)$ dependence coefficients and provides further evidence of the existence of the 5 dependence subgroups identified in our exploratory analysis for challenge C4. It also suggests that between group independence as well as within group asymptotic independence – in the sense that the extremes of within group variables do not occur simultaneously – are both reasonable modelling assumptions.

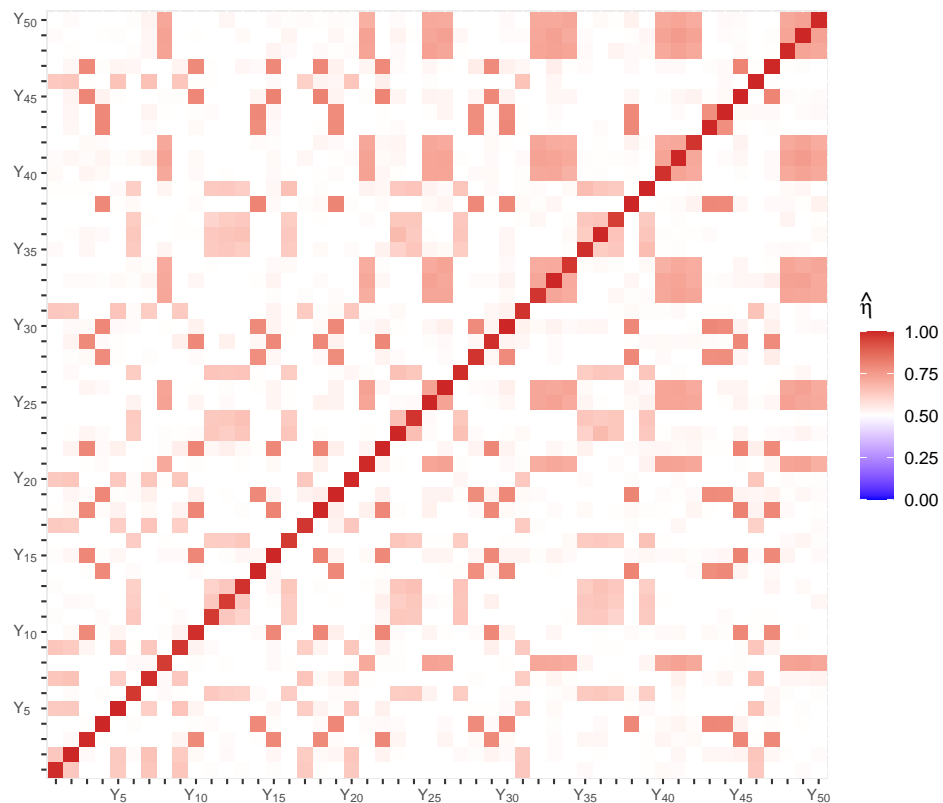


Figure S17: Heat map of estimated empirical pairwise $\eta(u)$ extremal dependence coefficients with $u = 0.95$.

Figure S18 shows the bootstrapped estimated individual group and overall probabilities with respect to conditioning threshold quantile for part 2 of challenge C4.

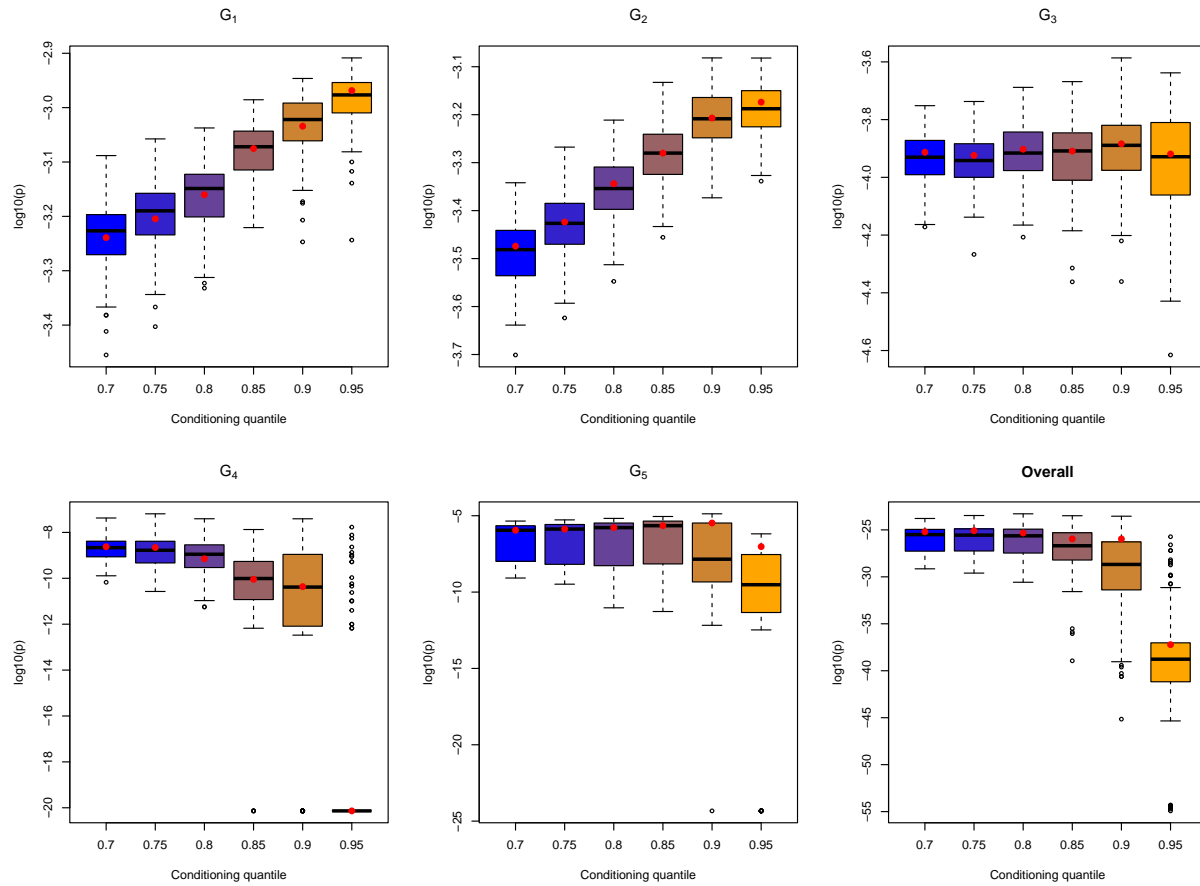


Figure S18: Part 2 subgroup and overall bootstrapped probability estimates on the log scale for C4. The red points indicate the original sample estimates and the colouring of the boxplots indicates the choice of conditioning threshold, with the conditioning quantile indices 1-6 referring to the quantile levels $\{0.7, 0.75, 0.8, 0.85, 0.9, 0.95\}$, respectively.